Dr. K. C. Tiwari

Rakeshmodi_24ginf03Mtech(Satellite Image Change Detection for Assessing Air Pollution–Climate __Interactions over Delhi)

PAPER

Document Details

Submission ID
trn:oid:::27535:142575539

Submission Date
Jun 11, 2026, 12:08 PM GMT+5:30

Download Date
Jun 11, 2026, 12:16 PM GMT+5:30

File Name
Rakeshmodi_24ginf03Mtech(Satellite Image Change Detection for Assessing Air Pollution–Climat....pdf

File Size
6.4 MB

58 Pages

11,833 Words

65,635 Characters

6% Overall Similarity

The combined total of all matches, including overlapping sources, for each database.

Exclusions

- 85 Excluded Matches

Match Groups

31 Not Cited or Quoted 2%
Matches with neither in-text citation nor quotation marks

37 Missing Quotations 4%
Matches that are still very similar to source material

1 Missing Citation 0%
Matches that have quotation marks, but no in-text citation

0 Cited and Quoted 0%
Matches with in-text citation present, but no quotation marks

Top Sources

3% Internet sources
2% Publications
5% Submitted works (Student Papers)

Match Groups

- **31** Not Cited or Quoted 2%
  Matches with neither in-text citation nor quotation marks
- **37** Missing Quotations 4%
  Matches that are still very similar to source material
- **1** Missing Citation 0%
  Matches that have quotation marks, but no in-text citation
- **0** Cited and Quoted 0%
  Matches with in-text citation present, but no quotation marks

Top Sources

3% Internet sources
2% Publications
5% Submitted works (Student Papers)

Top Sources

The sources with the highest number of matches within the submission. Overlapping sources will not be displayed.

1	Student papers	
Motilal Nehru National Institute of Technology on 2026-04-17		2%
2	Internet	
www.frontiersin.org		<1%
3	Student papers	
Indian Institute of Technology, Madras on 2018-01-30		<1%
4	Internet	
link.springer.com		<1%
5	Internet	
blogs.shu.edu		<1%
6	Internet	
doaj.org		<1%
7	Internet	
agribalkan.congress.gen.tr		<1%
8	Student papers	
Higher Education Commission Pakistan on 2026-05-13		<1%
9	Student papers	
Higher Education Commission Pakistan on 2026-05-19		<1%
10	Student papers	
University of Southampton on 2012-03-12		<1%

11 Internet
www.ijeat.org <1%

12 Internet
www.ngndai.mnnit.ac.in <1%

13 Internet
eprints.utar.edu.my <1%

14 Publication
Hafiz Humza Khalid, Ze-hui Li, Hong-di He, Hafiz Muhammad Hazib, Zhong-ren Pe... <1%

15 Internet
www.mdpi.com <1%

16 Publication
Aznarul Islam, Debajit Datta, Biplab Sarkar, Sandipan Ghosh, Sanat Kumar Guchh... <1%

17 Student papers
Brunel University on 2026-01-07 <1%

18 Student papers
Indian Institute of Information Technology and Management, IIITKM, Trivandru... <1%

19 Student papers
The University of Manchester on 2025-08-26 <1%

20 Publication
Xuedong Lin. "The trend on runoff variations in the Lhasa River Basin", Journal of ... <1%

21 Internet
wjarr.com <1%

22 Publication
David P. Turner. "Site-level evaluation of satellite-based global terrestrial gross pr... <1%

23 Publication
Fenglin Han, Sri Harsha Kota, Yungang Wang, Hongliang Zhang. "Source apportio... <1%

24 Student papers
Kenyatta University on 2017-05-24 <1%

25 Student papers
School of Planning and Architecture on 2025-04-04 <1%

26 Publication
Shi-Wei Li, Minghui Chang, Huiming Li, Xin-Yi Cui, Lena Q. Ma. "Chemical composi... <1%

27 Student papers
University of Hong Kong on 2025-05-13 <1%

28 Internet
ebin.pub <1%

29 Internet
kuscholarworks.ku.edu <1%

30 Internet
mdpi-res.com <1%

31 Internet
ugspace.ug.edu.gh <1%

32 Student papers
The Hong Kong Polytechnic University on 2014-01-26 <1%

33 Internet
www.thesocialbrooklyn.com <1%

34 Publication
Jesús Gonzalo. "Space Technology for Disaster Monitoring, Mitigation and Damag... <1%

35 Publication
Srinivas Yerramsetti, Manish Anand. "Chapter 9 Reconciling Value Trade-Offs in A... <1%

36 Student papers
The Energy and Resources Institute on 2015-01-16 <1%

37 Student papers
The University of Manchester on 2017-09-01 <1%

38 Student papers
University of Aberdeen on 2026-01-03 <1%

39 Student papers

Aligarh Muslim University, Aligarh on 2025-06-17 <1%

40 Internet

articles.economictimes.indiatimes.com <1%

21

CHAPTER 1

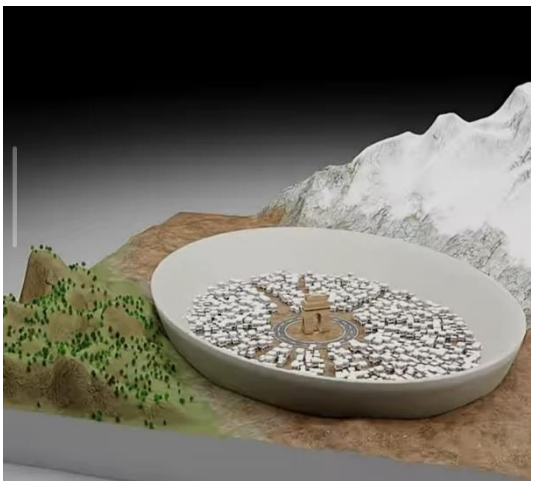
INTRODUCTION

1.1 Background and Motivation

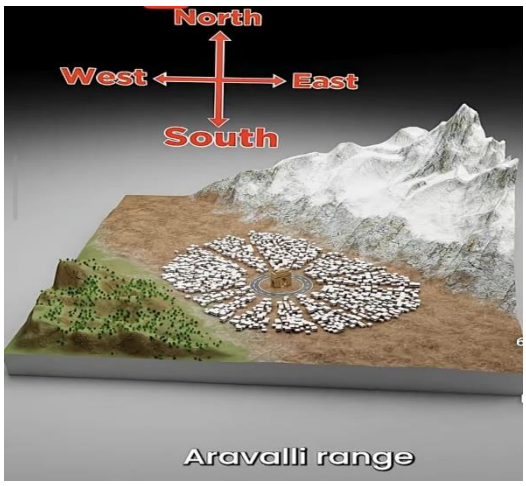
33

Air pollution is among the foremost environmental and public health crises of the 21st century. The World Health Organization (WHO, 2024) estimates that ambient fine particulate matter (PM2.5) pollution causes approximately 7 million premature deaths annually — more than HIV/AIDS, tuberculosis, and malaria combined. Delhi, the capital of India and anchor of the 46-million-strong National Capital Region (NCR), has consistently ranked among the world's most polluted cities, recording average annual PM2.5 concentrations of 89.1 µg/m³ in 2024 — 17.8 times the WHO annual guideline of 5 µg/m³ (IQAir, 2025). During severe winter smog events, 24-hour PM2.5 concentrations have exceeded 900 µg/m³, a 180-fold exceedance of WHO guidelines.

The IPCC AR6 (2021) has explicitly identified South Asian megacities — particularly those on the Indo-Gangetic Plain (IGP) — global pollution hotspots where air quality and climate interact through multiple feedback mechanisms. Delhi's crisis is uniquely complex owing to the convergence of four factors: (1) a multi-source emission structure spanning transport, industry, biomass burning, and dust; (2) a geographic pollution trap formed by the Himalayas to the north-northeast and Aravalli Range to the southwest; (3) seasonal atmospheric inversions that collapse the planetary boundary layer (PBL) to 100–300 m in winter; and (4) transboundary crop residue burning (CRB) aerosol transport from Punjab and Haryana via northwesterly wind corridors.



[Fig. 1.1: The Delhi 'bowl' — enclosed by Himalayas (NE) and Aravalli Range (SW). Source: Study illustrations.]



[Fig. 1.2: Geographic orientation of Delhi NCR in the Indo-Gangetic Plain. Source: Study illustrations.]

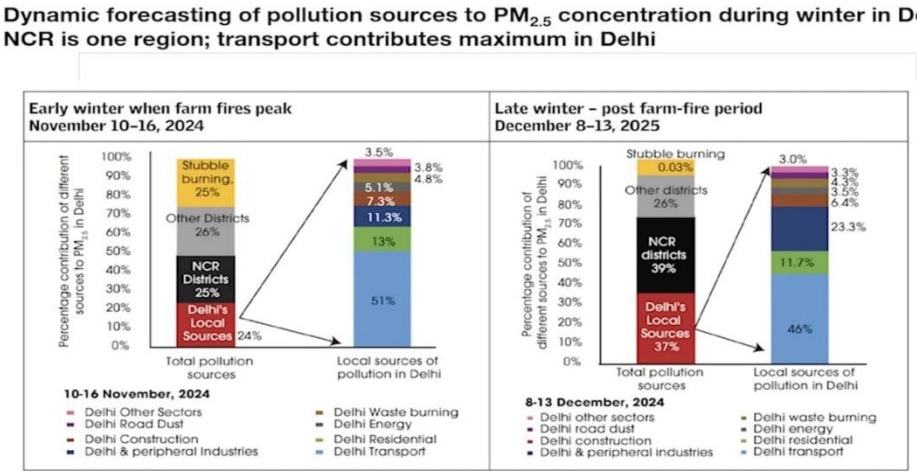
Satellite remote sensing — particularly the MODIS instruments aboard NASA's Terra and Aqua satellites — has provided continuous, calibrated, freely accessible observations since 2000, enabling 20-year analysis of these interactions at 1 km spatial resolution. Google Earth Engine (GEE) has democratised access to these petabyte-scale archives, enabling cloud-based processing without local computational

infrastructure. This study harnesses these capabilities for a comprehensive spatio-temporal analysis of Delhi NCR's air pollution–climate system.

1.2 Delhi's Pollution Sources: A Multi-Origin Structure

The source apportionment of PM2.5 in Delhi reveals a complex multi-origin structure. At the regional scale, approximately 70% of Delhi's total pollution load originates outside city boundaries — from NCR districts (35%), other states (27%), and stubble burning in Punjab/Haryana (8%). The remaining 30% is locally generated. Of locally generated pollution, transport dominates at 51%, followed by residential sources (13%), peripheral industries (11%), construction (7%), energy production (5%), waste burning (5%), road dust (4%), and others (4%) (CSE/IITM DSS, 2024).

This source structure has profound policy implications: measures targeting only one source — for example, stubble burning bans without addressing vehicular emissions — will have limited impact on Delhi's overall pollution burden. During early winter when farm fires peak (November 10–16), stubble burning contributes 25% of total pollution; by late winter (December 8–13), this falls to 0.03% while transport remains consistently dominant at 46%.



[Fig. 1.3: Dynamic PM2.5 source forecast — early winter vs late winter. Source: CSE/IITM DSS, 2024.]

1.3 The Crop Residue Burning Problem

Crop residue burning (CRB) — locally known as 'parali' burning — is the seasonal practice of burning paddy straw after the Kharif (rice) harvest in October–November, and wheat straw after the Rabi harvest in April–May. Satellite-based fire detection consistently shows that Punjab generates 92.58% and Haryana 7.42% of regional stubble burning activity in November (Das et al., 2024).

The root cause is well-established: the Punjab Preservation of Subsoil Water Act, 2009 (Punjab Act No. 6 of 2009) prohibits paddy transplantation before the government-notified date (typically 10–15 June). This water conservation measure compresses the paddy cultivation season, leaving insufficient time between rice harvest (late October) and wheat sowing (November) for mechanised residue management. As a consequence, burning — quick, cheap, and labour-free — remains the default option for small and marginal farmers (Erbaugh et al., 2024).

However, recent research has complicated the dominant CRB narrative. Kundu et al. (2025, npj Climate and Atmospheric Science) demonstrate weak coupling between observed surface PM2.5 in Delhi-NCR and rice crop residue burning in Punjab and Haryana, showing that while satellite-visible plumes are extensive, their contribution to ground-level PM2.5 in Delhi is estimated at only 8–25% during peak burning. Graham et al. (2024) applied HYSPLIT back-trajectory modelling and confirmed that aerosol plumes originating from Punjab burning zones reach Delhi in approximately 15–16 hours under northwesterly flow. This transport timeline is independently corroborated in the present study by the satellite-detected northwest-to-southeast AOD gradient across the 18 NCR districts, with the three highest ΔAOD values concentrated in districts directly exposed to northwesterly advection (Shahdara, North East, Baghpat; Section 6.3).

1.4 Wind Transport Mechanisms

Wind patterns are the critical link between the Punjab/Haryana stubble-burning source region and Delhi as the receptor. The prevailing northwesterly winds during October–November carry smoke, particulates, and gaseous pollutants from burning fields in south Punjab directly toward Delhi. Graham et al. (2024) used HYSPLIT back-trajectory modelling to show that air masses originating in the Punjab burning zone can reach Delhi in as little as 15–16 hours, arriving during pre-dawn hours when the planetary boundary layer is at its shallowest. While HYSPLIT trajectory simulation falls outside the scope of this satellite-only study, the northwesterly transport hypothesis is supported by the spatial pattern of district-level AOD enhancement observed here, where the steepest pollution increases occur in the districts that receive northwesterly flow first (Section 6.3).

Wind speed is as important as direction. Near-calm winds (< 2 m/s) during November–December nights create the worst pollution episodes. The November 2023–24 average surface wind speed was approximately 9.8 m/s — about 21% slower than the six-year mean — contributing to record high AOD values recorded that year. Long-term global warming is also expected to weaken IGP surface winds, systematically worsening Delhi's pollution carrying capacity independent of emission trends (Down to Earth, 2024).

1.5 Geographic Trapping — The Delhi Bowl

Delhi's geography has been described as a 'pollution trap' or 'bowl' — the convergence of topographic and meteorological factors that prevent escape of pollutants. The Himalayas, forming a massive wall to the north-northeast, block northward advection of surface-level pollution. The Aravalli Hills, running SW–NE along Delhi's western flank, offer only partial ventilation due to their low elevation and fragmented structure. The Shivalik foothills close off the NE escape route.

The critical mechanism is the temperature inversion — a meteorological condition where a warm air layer sits above cooler surface air, acting as a lid preventing vertical mixing. In winter, radiative cooling of the surface at night creates stable stratification. With the PBL compressed to 100–300 m, all ground-level emissions are concentrated into a shallow layer at breathing height. The mixing height varies from ~100 m on winter nights to ~1,000 m in summer — a 10-fold range that drives the extreme seasonality of Delhi's pollution, more powerfully than emission seasonality alone (Guttikunda and Gurjar, 2012).

1.6 The Waste Burning Crisis

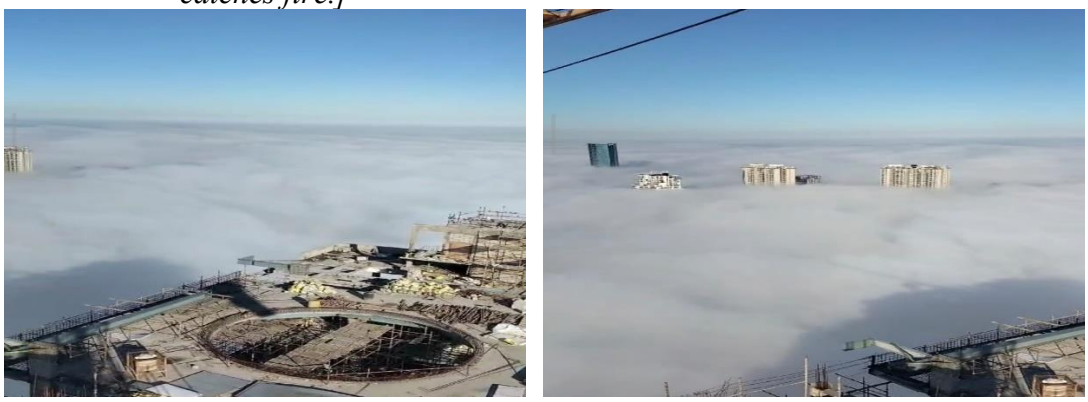
25 Delhi operates three major landfill sites — Bhalswa, Ghazipur, and Okhla — that have become symbols of urban waste management failure. Ghazipur landfill, standing over 65 metres tall, regularly catches fire, releasing toxic black carbon, dioxins, and PM2.5 at ground level into surrounding residential areas. Scientific estimates indicate that total Municipal Solid Waste (MSW) burned in Delhi ranges from 190–246 tonnes per day (Nagpure et al., 2015), contributing approximately 5% of locally generated PM2.5.



[Fig. 1.4: Ghazipur landfill mountain, Delhi -over 65 metres tall, frequently catches fire.]



[Fig. 1.5: Ghazipur landfill on fire with fire services.]



[Fig. 1.6: Delhi's smog layer from above — thermal inversion lid visible.]

18 ## 1.7 Research Objectives

This study has the following specific research objectives:

1. Quantify the spatio-temporal change in Aerosol Optical Depth (AOD) across 18 districts of Delhi NCR between the baseline period (2005–09) and the current period (2020-24) using MODIS MAIAC MCD19A2 data at 1 km resolution.
2. Assess the change in Land Surface Temperature (LST) and identify the aerosol radiative dimming effect through AOD-LST Pearson correlation analysis across three seasons.
3. Analyse vegetation dynamics (NDVI) to determine greening/browning trends and their relationship with high-AOD districts.

19

4. Quantify long-term AOD trend rates using Sen's Slope analysis and Mann–Kendall significance testing at per-pixel resolution.
5. Perform ground-level validation of satellite-derived AOD against CPCB station AQI data (2019–2024) from 11 Delhi NCT districts.
6. Critically synthesise peer-reviewed literature on crop residue burning, wind transport mechanisms, geographic trapping, and evidence-based mitigation strategies.
7. Provide a replicable, cloud-based GEE + Python + ArcGIS framework applicable for operational air quality monitoring.

CHAPTER 2

LITERATURE REVIEW

2.1 Satellite-Based AOD Studies in Delhi NCR

Aerosol Optical Depth has been extensively validated as a proxy for column aerosol loading and ground-level PM2.5 concentrations. For the Indian subcontinent, Dey and Di Girolamo (2010) demonstrated statistically significant correlations between MODIS AOD and AERONET station data. The MODIS MAIAC (Multi-Angle Implementation of Atmospheric Correction) algorithm used in MCD19A2 represents a significant methodological advancement, employing time-series surface reflectance modelling to achieve retrievals over bright urban surfaces at 1 km resolution (Lyapustin et al., 2011).

Kaskaoutis et al. (2014) identified distinct seasonal AOD patterns over Delhi: lowest in winter, highest in pre-monsoon (dust storms), and a secondary post-monsoon peak from agricultural burning. Jethva et al. (2019), using a 15-year MODIS record, established a net ~60% increase in post-harvest fire activity and a 43% increase in regional aerosol loading over the IGP (2002–2016). Thakur et al. (2025) confirmed that the COVID-19 lockdown produced a significant but short-lived AOD reduction followed by complete rebound — a pattern fully reproduced in the present study.

2.2 Crop Burning, Wind Transport and the CRB Debate

Das et al. (2024) confirmed Punjab's dominance (92.58%) in regional burning activity using MODIS FIRMS and Sentinel-5P TROPOMI CO/NO2. Graham et al. (2024), published in Atmospheric Chemistry and Physics, combined TROPOMI tropospheric column NO2 with ROTRAJ back-trajectory modelling to establish that non-local transport emissions dominate (>75%) on high-pollution days with northwesterly winds, with transit times of only 15–16 hours. Singh et al. (2023) used a 29-station CUPI-G sensor network and tracked PM2.5 plumes exceeding 500 µg/m³ from Punjab to Delhi with transit delays of 1–3 days.

A critical counter-narrative emerged from Kundu et al. (2025), who found weak coupling between Delhi-NCR PM2.5 and fire detection counts over Punjab/Haryana during 2015–2023. While fire counts declined by more than 50%, Delhi PM2.5 remained persistently elevated — demonstrating that structural emission sources dominate and that stubble-burning bans alone cannot resolve Delhi's chronic pollution. Biswal et al. (2025) added nuance by showing that evening CRB, coinciding with PBL collapse, produces threefold higher Delhi PM2.5 than daytime burning.

Table 2.1 Key peer-reviewed studies on CRB, wind transport and Delhi air quality (2019–2026)

Study	Method	Period	Key Finding
Jethva et al. (2019)	MODIS AOD + NDVI; 15-yr	2002–16	+60% fire; +43% IGP AOD
Das et al. (2024)	MODIS FIRMS + TROPOMI	2020–21	Punjab = 92.58% of Nov CRB
Graham et al. (2024)	TROPOMI + ROTRAJ traj.	2017–20	>75% non-local; 15–16 hr transit

Singh et al. (2023)	29-station network + HYSPLIT	Oct–Nov 22	PM2.5 >500 µg/m³ plumes tracked
Kundu et al. (2025a)	Sensors + dispersion model	2015–23	CRB ~14% Delhi PM2.5; FDC fell 50%
Kundu et al. (2025b)	Multi-model PM2.5 + FDC	2015–23	Weak CRB–PM2.5 coupling confirmed
Biswal et al. (2025)	Emission timing analysis	2022–24	Evening CRB → 3× higher PM2.5
Thakur et al. (2025)	Geospatial + AQI; COVID	2018–23	COVID AOD −14%; rebound 2021
Beig et al. (2023)	MODIS + ERA-5 + HYSPLIT	Oct–Nov 22	AOD ×4 above pre-burning baseline
Nirwan et al. (2024)	TROPOMI CO/NO2/SO2 + CAMS	2018–22	SE Punjab 111 km² = CO hotspot

2.3 Aerosol Radiative Forcing and Land Surface Temperature

The aerosol solar-dimming effect was first systematically studied at global scale by Ramanathan et al. (2001) and Wild et al. (2005). For the Indo-Gangetic Plain, Bollasina et al. (2011) showed that the South Asian Brown Cloud reduces surface solar radiation by 10–15 W/m² and suppresses monsoon precipitation. Mohan and Kandya (2015) quantified Urban Heat Island intensities of 2–4°C in Delhi using MODIS MOD11A1. The competition between UHI warming and aerosol dimming cooling, and its spatial distribution across 18 NCR districts, is one of the primary contributions of the present study.

2.4 Vegetation Dynamics and NDVI

Numerous studies have documented a global greening trend using MODIS NDVI data (Zhu et al., 2016), attributable to CO2 fertilisation, nitrogen deposition, and warming growing seasons. Delhi's green cover expanded from approximately 22 km² in 1993 to an estimated 342 km² in 2021 (FSI ISFR 2021). However, Garg et al. (2019) cautioned that NDVI improvements do not translate to proportional air quality improvements, as urban vegetation has limited capacity to intercept fine particles (PM2.5) compared to coarser PM10.

2.5 Source Apportionment Studies

Source apportionment studies for Delhi employ receptor modelling (PMF, CMB), chemical transport models (WRF-Chem, CHIMERE), and isotopic analysis. The IITM Decision Support System integrates PMF output with CHIMERE-WRF chemical transport modelling to produce dynamic daily source apportionment used operationally by CAQM. Key findings from CSE (2024) establish that transport is the dominant local source in all seasons, contributing 46–51% of locally generated PM2.5. Municipal solid waste burning contributes 190–246 tonnes/day (Nagpure et al., 2015), approximately 5% of local PM2.5.

2.6 Policy Interventions — India and International Comparison

China's 'Action Plan on Prevention and Control of Air Pollution' (2013–2017) achieved PM2.5 reductions of 33% in Beijing over four years through coal-to-gas fuel switching, steel capacity cuts, and stricter vehicle emission standards (Zheng et al.,

2018). India's National Clean Air Programme (NCAP, 2019) targeted 20–30% PM reduction by 2024, but CSE audits show less than 1% of NCAP funds were spent on industrial emission controls, with approximately 40% of allocated Rs. 10,566 crores remaining unspent — underscoring the gap between policy intent and implementation.

2.7 Research Gaps Addressed by This Study

The literature reviewed in Sections 2.1 to 2.6 reveals three gaps that the present study is specifically designed to fill.

First, no prior study has simultaneously tracked 20-year trends in AOD, LST, and NDVI across all 18 administrative districts of Delhi NCR within a single unified analytical framework. Existing work either focuses on a single parameter such as AOD (Kaskaoutis et al., 2014; Jethva et al., 2019), covers limited time periods, or operates at spatial scales too coarse for district-level policy differentiation. The absence of an integrated multi-variable, long-term, district-resolution analysis represents a significant gap given that pollution drivers, vegetation cover, and thermal environments vary substantially across the NCR's urban core, peri-urban belt, and rural periphery.

24

Second, while the aerosol direct radiative effect has been quantified at regional and global scales (Ramanathan et al., 2001; Bollasina et al., 2011), its spatial manifestation at 1 km resolution across Delhi NCR's districts — and particularly the spatial competition between aerosol solar-dimming cooling and urban heat island warming — has not been systematically mapped using two decades of satellite data. It remains unclear which districts experience net cooling from aerosols and which remain dominated by urbanisation-driven warming.

Third, Delhi's large-scale afforestation programme has produced measurable NDVI increases in parts of the NCR, yet this greening trend has developed alongside simultaneously worsening AOD. The spatial decoupling between vegetation improvement and air quality deterioration at the district level, and the extent to which aerosol-induced suppression of photosynthetically active radiation limits vegetation health in high-pollution districts, has not been characterised at satellite resolution.

This study addresses all three gaps through the integrated GEE and Python-based change detection framework described in Chapter 5, using five satellite products spanning 2005–2024.

"These identified gaps directly motivate the seven research objectives outlined in Section 1.7, which this study addresses through a 20-year satellite-based analysis."

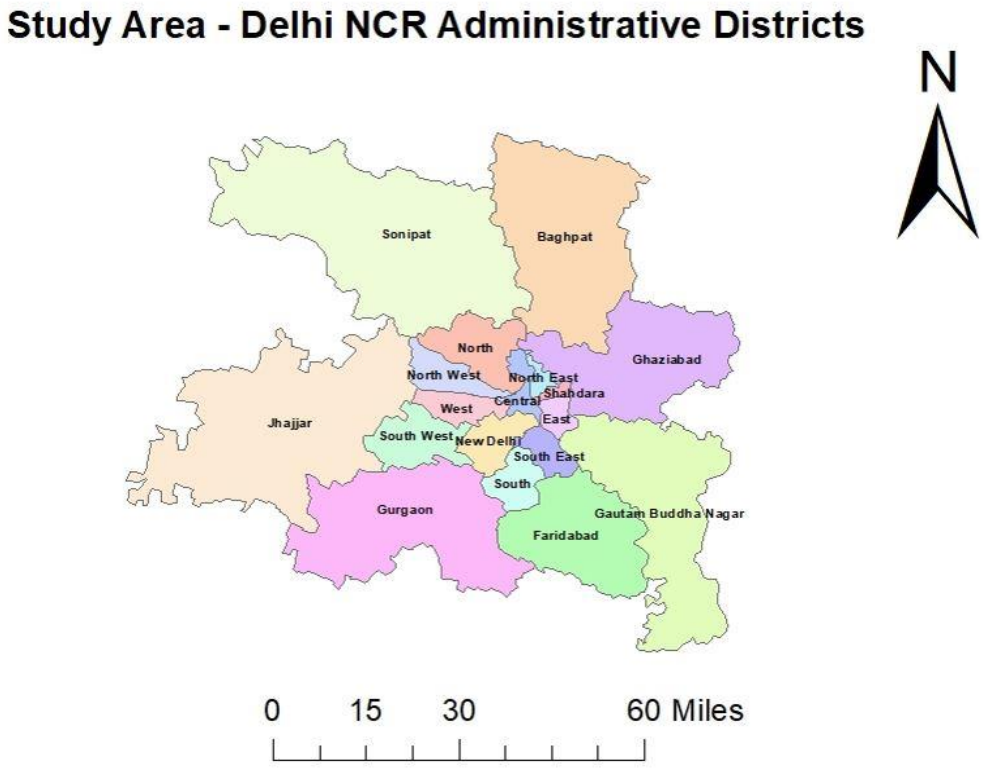
CHAPTER 3

STUDY AREA

3.1 Geographic Setting of Delhi NCR

The study area encompasses the Delhi National Capital Territory (NCT) and the National Capital Region (NCR), situated between 28.08°N–29.30°N latitude and 76.28°E–77.72°E longitude, covering approximately 55,083 km² at approximately 228 m AMSL on the flat Indo-Gangetic alluvial plain. The terrain is uniformly flat, underlain by Quaternary alluvial sediments deposited by the Yamuna and other rivers draining the Himalayas, providing no topographic barriers to pollutant transport within the basin.

Delhi's geographic position creates a natural pollution trap at multiple scales. At macro-scale, the Himalayas (2,000–8,000 m elevation) form an impenetrable northern wall preventing northward advection of surface-level pollution. The Aravalli Hills (300–600 m), one of the world's oldest mountain ranges, partially block westerly flow from the south-west but are insufficiently high and continuous to prevent all pollution transport. The open IGP corridor to the northwest creates the primary pollution transport highway from Punjab and Haryana, channelling crop-burning aerosols directly toward Delhi under northwesterly flow.



[Fig. 3.1: Study area map — 18 administrative districts of Delhi NCR. Coordinates: 28.08°N–29.30°N, 76.28°E–77.72°E. Source: ArcGIS 10.8, this study.]

3.2 Administrative Districts

Table 3.1 Administrative districts of Delhi NCR included in this study

District	State	Area (km²)	Population	Pollution Characteristics
New Delhi	Delhi NCT	42.7	142,004	Administrative core; sheltered
North	Delhi NCT	60.3	885,000	Dense residential; vehicular
North West	Delhi NCT	440	3,657,000	Mixed industrial-residential
North East	Delhi NCT	60	2,213,000	Highest density; NW corridor entry
East	Delhi NCT	64	1,447,000	Dense urban; Yamuna riverside
Shahdara	Delhi NCT	245	1,729,000	Highest ΔAOD; NW corridor
West	Delhi NCT	129	2,543,000	Pusa-Shadipur industrial
Central	Delhi NCT	24.7	579,000	Commercial core
South	Delhi NCT	250	2,731,000	Residential; Aravalli proximity
South West	Delhi NCT	420	2,549,000	Airport; Dwarka residential
South East	Delhi NCT	35	500,000	Okhla industrial area
Gurgaon	Haryana	1,253	1,514,000	IT hub; NCR growth centre
Jhajjar	Haryana	1,834	956,000	Agricultural; peri-urban
Sonipat	Haryana	2,122	1,451,000	Industrial; Haryana border
Faridabad	Haryana	742	1,798,000	Heavy industry south
Baghpat	UP	1,321	1,303,000	Agricultural; UP border
Ghaziabad	UP	1,179	4,681,000	Industrial; transport hub
Gautam Buddha Nagar	UP	1,441	1,648,000	Noida; IT/ITES sector

3.3 Climate and Seasonal Dynamics

Delhi has a semi-arid climate (BSh in Köppen classification) with extreme seasonal temperature variation. Annual mean temperature is approximately 25°C, with January means of ~13°C and May means of ~36°C. Annual rainfall averages 714 mm, concentrated in the southwest monsoon (June–September). This study analyses three seasons chosen for their distinct pollution dynamics, as defined below.

Table 3.2 Seasonal climate characteristics of Delhi NCR

Season	Months	Temp (°C)	Mean AOD	Key Pollution Drivers
Post-Monsoon	Nov–Dec	18–28°C	0.984	Peak CRB; northwesterly winds; worst PM2.5
Winter	Jan–Feb	12–20°C	0.729	Deep inversions; PBL ~100 m; fog; local vehicle
Pre-Monsoon	Jun–Jul	35–42°C	0.952	Dust storms from Thar Desert; convective mixing
Monsoon (ref.)	Jul–Sep	28–35°C	~0.5	Wet deposition cleans aerosols; not analysed

3.4 The Planetary Boundary Layer Problem

The critical physical mechanism driving Delhi's winter pollution severity is the collapse of the planetary boundary layer (PBL). The mixing height determines the

atmospheric volume available for pollutant dilution. In winter, radiative cooling at night collapses the PBL to just 100–200 metres — equivalent to a 30-storey building. All emissions from vehicles, industries, waste burning, and stubble smoke are compressed into this thin slab at breathing height, producing PM2.5 concentrations routinely exceeding 300 µg/m³ during the most severe episodes.

This 10-fold seasonal range in mixing height (100 m to 1,000 m) explains Delhi's extreme air quality seasonality more powerfully than emission seasonality alone (Guttikunda and Gurjar, 2012). Even with constant emission rates, a 10-fold reduction in PBL height produces a 10-fold increase in ground-level PM2.5 concentration, following the basic dilution relationship:

$$C_surface = E / (u \times H \times W) \quad (3.1)$$

where C is surface concentration, E is emission rate, u is wind speed, H is mixing height, and W is the dilution width.

Table 3.3 Seasonal mixing layer height and pollution implications for Delhi NCR

Season/Period	Typical Mixing Height	Air Quality Implication
Winter nights (Dec–Feb)	~100 m	Catastrophic; PM2.5 > 300 µg/m³; 60× WHO annual
Winter days (Dec–Feb)	~200–400 m	Highly polluted; all NAAQS exceedances
Post-Monsoon (Oct–Nov)	~400–600 m	Stubble burning peak; severe despite taller MLH
Pre-Monsoon (Apr–Jun)	~600–900 m	Dust storms dominate; moderate pollution
Monsoon (Jul–Sep)	~1000-1500 m	Best air quality; monsoon cleansing

3.5 Source Regions and Wind Transport Corridors

The primary CRB source regions lie 200–500 km to the northwest of Delhi in Punjab (area: 50,362 km²) and Haryana (44,212 km²). Punjab's Malwa region and the Punjab–Haryana border belt consistently generate the highest fire counts per km². The seasonal wind regime is driven by the retreat of the ITCZ southward in October, which shifts circulation from southwesterly monsoon winds to northwesterly post-monsoon flow. This transport corridor passes over Ludhiana, Ambala, Kurukshetra, Karnal, and Panipat — all significant emission sources — adding further pollution to advecting plumes.

Table 3.4 Seasonal wind dynamics and pollution characteristics for Delhi NCR

Season	Wind Direction	Speed (m/s)	PBL (m)	Dominant Source
Post-Monsoon	Northwesterly (>75% of high-pollution days)	2–8	100–400	CRB + local transport + industrial
Winter	Variable; often calm (<2 m/s)	1–5	100–300	Local transport + industrial + fog
Pre-Monsoon	SW + NW dust	10–25	800–1200	Thar Desert dust + vehicular
Monsoon	Southwesterly	15–30	1000–1500	Wet deposition cleans aerosols

CHAPTER 4

THEORETICAL FRAMEWORK

4.1 Aerosol Optical Depth — Physical Principles

Aerosol Optical Depth (AOD) is a dimensionless, column-integrated measure of the extinction (scattering + absorption) of solar radiation by suspended aerosol particles. It is defined by the Beer-Lambert Law:

$$I(\lambda) = I_0(\lambda) \cdot \exp(-\tau(\lambda) / \cos\theta) \quad (4.1)$$

where I(λ) is the measured radiance at wavelength λ, $I_0(\lambda)$ is the extra-atmospheric solar radiance, τ(λ) is the AOD at wavelength λ, and θ is the solar zenith angle. MODIS retrieves AOD at 550 nm. The MAIAC algorithm (MCD19A2) applies a time-series surface reflectance model:

$$\rho_TOA(\lambda, \theta) = f[\rho_surface(\lambda, \Omega), \tau_aerosol(\lambda), P_aerosol, \tau_gas(\lambda)] \quad (4.2)$$

The MODIS AOD uncertainty is ±0.05 + 15% over land (Lyapustin et al., 2018). Scale conversion from raw digital number to physical AOD:

$$AOD = Raw_pixel_value \times 0.001 \quad (4.3)$$

AOD > 1.0 is internationally recognised as the hazardous threshold, corresponding approximately to PM2.5 concentrations exceeding 75 µg/m³.

Table 4.1 AOD classification thresholds and approximate PM2.5 equivalents

AOD Value	Air Quality	PM2.5 (µg/m³)	Health Implication
< 0.1	Very Clean	< 10	Pristine; background conditions
0.1–0.5	Clean–Moderate	10–50	Normal urban; some haze
0.5–1.0	Polluted	50–100	Visible haze; health concern
> 1.0	Hazardous	> 100	Severe health risk; emergency levels

4.2 Land Surface Temperature — Split-Window Algorithm

Land Surface Temperature (LST) is the radiometric temperature of the uppermost land surface layer. MODIS MOD11A1 retrieves LST using the Split-Window Algorithm (SWA) applied to thermal infrared channels 31 (10.78–11.28 µm) and 32 (11.77–12.27 µm):

$$LST = A_0 + A_1 T_{31} + A_2 T_{32} + A_3 (T_{31} - T_{32}) \quad (4.4)$$

where T_{31} and T_{32} are brightness temperatures in channels 31 and 32, and A_0–A_3 are regression coefficients depending on atmospheric water vapour and surface emissivity. Accuracy: ±1°C under clear-sky conditions (Wan, 2014). The scale conversion from raw DN to physical temperature:

$$LST\ (°C) = Raw_pixel_value \times 0.02 - 273.15 \quad (4.5)$$

4.3 Normalised Difference Vegetation Index

The NDVI exploits the spectral contrast between healthy green vegetation (high NIR reflectance, low red reflectance) and non-vegetated surfaces. First proposed by Rouse et al. (1974):

$$NDVI = (\rho_NIR - \rho_RED) / (\rho_NIR + \rho_RED) \quad (4.6)$$

where ρ_NIR is surface reflectance in MODIS Band 2 (841–876 nm) and ρ_RED is surface reflectance in Band 1 (620–670 nm). NDVI ranges from −1 (open water) through 0 (bare soil) to +1 (dense healthy vegetation). Scale conversion:

$$NDVI = Raw_pixel_value \times 0.0001 \quad (4.7)$$

4.4 Geographic Trapping Mechanism

The geographic configuration of Delhi creates a natural pollution trap operating at multiple scales. At macro-scale, the Himalayas form an impenetrable northern wall preventing northward advection. The Aravalli Hills partially block western flow but are too low and discontinuous to prevent all outflow. At mesoscale, the open IGP corridor to the northwest functions as the primary pollution import highway from Punjab and Haryana. Under calm anticyclonic conditions, multiple source region contributions accumulate simultaneously within the Delhi bowl, producing the compound pollution episodes characteristic of November–December.

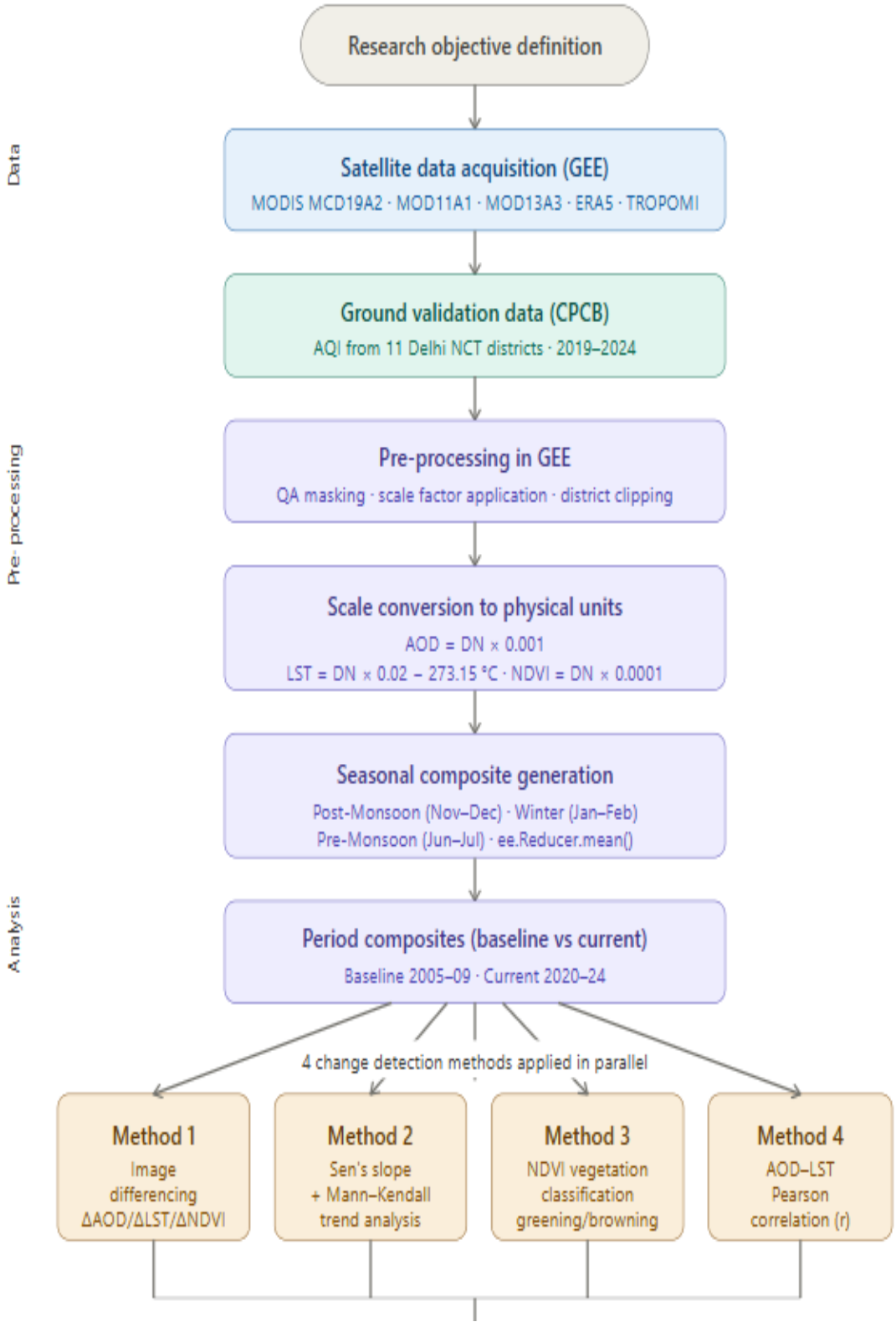
4.5 Source Apportionment Framework

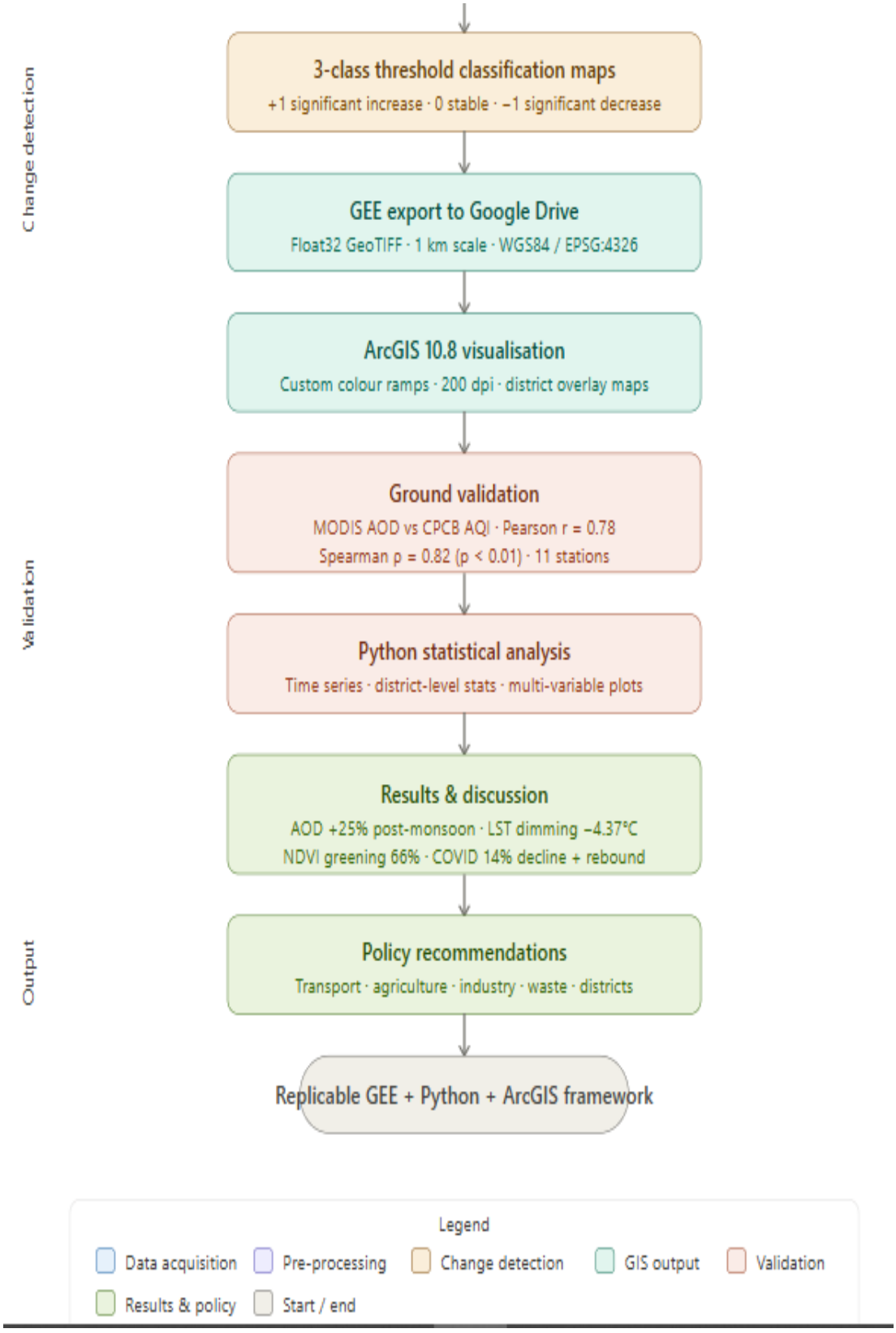
PM2.5 source apportionment employs the Positive Matrix Factorization (PMF) receptor model. The governing equation decomposes the measured concentration matrix as:

$$x(i,j) = \Sigma_k[g(i,k) \cdot f(k,j)] + e(i,j) \quad (4.8)$$

where x(i,j) is the concentration of species j in sample i, g(i,k) is the contribution of source k to sample i, f(k,j) is the source profile of species j in source k, and e(i,j) is the residual error. The IITM DSS integrates PMF output with CHIMERE-WRF chemical transport modelling to produce dynamic daily source apportionment used operationally by CAQM.

CHAPTER 5
DATA AND METHODOLOGY




Change detection
3-class threshold classification maps
+1 significant increase · 0 stable · −1 significant decrease
GEE export to Google Drive
Float32 GeoTIFF · 1 km scale · WGS84 / EPSG:4326
ArcGIS 10.8 visualisation
Custom colour ramps · 200 dpi · district overlay maps
Validation
Ground validation
MODIS AOD vs CPCB AQI · Pearson r = 0.78
Spearman ρ = 0.82 (p < 0.01) · 11 stations
Python statistical analysis
Time series · district-level stats · multi-variable plots
Results & discussion
AOD +25% post-monsoon · LST dimming −4.37°C
NDVI greening 66% · COVID 14% decline + rebound
Output
Policy recommendations
Transport · agriculture · industry · waste · districts
Replicable GEE + Python + ArcGIS framework
Legend
Data acquisition
Pre-processing
Change detection
GIS output
Validation
Results & policy
Start / end

5.1 Satellite Data Sources

Table 5.1 Primary satellite datasets used in this study — all accessed via Google Earth Engine

Product	Variable	Resolution	Scale Factor	GEE Dataset ID	Period
MODIS MCD19A2 (MAIAC)	AOD @ 550 nm	1 km / Daily	×0.001	MODIS/061/MCD19A2_GRANULES	2005–2024
MODIS MOD11A1 (Terra)	LST Daytime	1 km / Daily	×0.02−273.15	MODIS/061/MOD11A1	2005–2024
MODIS MOD13A3 (Terra)	NDVI	1 km / Monthly	×0.0001	MODIS/061/MOD13A3	2005–2024
MODIS MOD14A1 (FIRMS)	Active Fire	1 km / Daily	Conf. ≥ 50%	MODIS/006/MOD14A1	2005–2024
ERA5 (ECMWF)	Wind, BLH, Temp	~31 km / Hourly	N/A	ECMWF/ERA5_LAND/HOURLY	2005–2024
Sentinel-5P TROPOMI	Tropospheric NO2	3.5×5.5 km / Daily	QA ≥ 0.75	COPERNICUS/S5P/OFFL/L3_NO2	2018–2024

The MODIS MAIAC algorithm used in MCD19A2 represents the current state of the art for satellite AOD retrieval over complex urban surfaces. Unlike earlier Dark Target and Deep Blue algorithms, MAIAC employs time-series surface reflectance analysis to separate atmospheric from surface signals, achieving retrievals over bright urban surfaces at 1 km resolution (Lyapustin et al., 2011). Note: The year 2008 was excluded from the baseline period due to incomplete MCD19A2 granule availability in GEE for the Delhi region during the specific seasonal windows defined. The baseline period therefore covers 4 years: 2005, 2006, 2007, and 2009.

5.2 Ground Validation Data — CPCB

To validate satellite-derived AOD against ground-level air quality measurements, CPCB ambient air quality monitoring station data were incorporated for 11 Delhi NCT districts. Seasonal AQI data from 2019–2024 were compiled from official CPCB monitoring stations.

Table 5.2 CPCB monitoring stations used for ground validation

District	CPCB Stations	No. Stations
North	Burari Crossing, Jahangirpuri, Rohini, Wazirpur, North Campus DU	5
North West	Alipur, Bawana, Narela, Mundka, Punjabi Bagh	5
West	Ashok Vihar, Pusa, Shadipur, DTU	4
South West	Dwarka Sec-8, NSIT Dwarka, IGI Airport T3, Najafgarh	4
South	Okhla Phase-2, Sri Aurobindo Marg, Nehru Nagar, Dr. Karni Singh Range	4
Central	Mandir Marg, Chandni Chowk	2

New Delhi	Lodhi Road, JN Stadium, Maj. Dhyan Chand Stadium	3
East	Patparganj, Vivek Vihar, IHBAS Dilshad Garden	3
North East	Sonia Vihar, Anand Vihar	2
South East	Okhla Phase-2	1
Shahdara	Vivek Vihar, IHBAS	2

5.3 Scale Conversion Equations and Physical Basis

Raw MODIS digital number (DN) values are converted to physical units using product-specific scale factors:

$$AOD = Raw_pixel_value \times 0.001 \quad (5.1)$$

$$LST\ (°C) = Raw_pixel_value \times 0.02 - 273.15 \quad (5.2)$$

$$NDVI = Raw_pixel_value \times 0.0001 \quad (5.3)$$

Worked example — AOD: Raw DN = 850 → AOD = 0.850 (polluted; clean air ≈ 0.05–0.15). LST: Raw DN = 15,500 → LST = 15,500 × 0.02 − 273.15 = 36.85°C. A critical technical note: in ArcGIS 10.8, importing GEE-exported Float32 GeoTIFFs as Int8 causes the −1 classification value (significant decrease) to read as 0, corrupting change maps. This was resolved by explicitly using .toFloat() in GEE before export — a documented methodological contribution for operational practitioners.

5.4 Seasonal Window Design and Study Period

The study compares two composite periods: a baseline period (2005–09) and a current period (2020–24). Three seasonal windows were defined:

Table 5.3 Seasonal windows and physical rationale

Season	Months (DOY)	Physical Rationale
Post-Monsoon	Nov–Dec (DOY 305–365)	Peak CRB season; northwesterly winds; worst PM2.5 health episodes; AOD > 1.0
Winter	Jan–Feb (DOY 1–59)	Deep inversions (PBL ~100 m); fog; local vehicle/industrial dominant; coldest days
Pre-Monsoon	Jun–Jul (DOY 152–212)	Maximum dust loading from Thar Desert; highest temperatures

The southwest monsoon period (July–September) is deliberately excluded from the change detection analysis for three scientifically grounded reasons. First, intense monsoon rainfall acts as an efficient wet deposition mechanism, removing aerosols from the atmospheric column and reducing AOD across Delhi NCR to seasonal minima of approximately 0.3–0.5. These values fall well below the polluted threshold of AOD > 0.5 and are not representative of the chronic air quality conditions that this study is designed to characterise. Second, sustained cloud cover during the monsoon months causes extensive pixel masking in MODIS AOD retrievals, with valid pixel fractions often falling below 30% per monthly composite for the Delhi NCR domain — a sampling fraction too sparse for reliable multi-year trend analysis. Third, this exclusion is consistent with established methodology in the peer-reviewed literature for satellite aerosol studies over the Indo-Gangetic Plain: Kaskaoutis et al. (2014) explicitly exclude the monsoon season from their long-term MODIS AOD

trend analysis over Delhi on the same grounds, and Jethva et al. (2019) similarly restrict their 15-year fire and aerosol analysis to the post-monsoon burning season. Including monsoon months would dilute the pollution signal, introduce retrieval-gap artefacts, and reduce the comparability of this study's results with the existing literature.

5.5 Change Detection Methods

5.5.1 Method 1: Image Differencing

Image differencing is the simplest and most widely used change detection technique (Lu et al., 2004). A pixel-wise arithmetic difference between the current and baseline composites produces a signed difference image:

$$\Delta AOD = AOD_current(2020–24) - AOD_baseline(2005–09) \quad (5.4)$$

$$\Delta LST = LST_current - LST_baseline \quad (5.5)$$

$$\Delta NDVI = NDVI_current - NDVI_baseline \quad (5.6)$$

A threshold-based classification converts continuous difference values into 3-class change maps:

$$Class = +1 \ \ if\ \Delta > +threshold \ \ \ (significant\ increase) \quad (5.7)$$

$$Class = \ 0 \ \ if\ |\Delta| \leq threshold \ \ (stable\ /\ no\ change) \quad (5.8)$$

$$Class = -1 \ \ if\ \Delta < -threshold \ \ \ (significant\ decrease) \quad (5.9)$$

Table 5.4 Change detection thresholds and rationale

Variable	Threshold	Rationale
AOD	±0.05 AOD units	MODIS MAIAC retrieval uncertainty; ≈ ±5 µg/m³ PM2.5
LST	±1.0°C	MOD11A1 accuracy specification (Wan, 2014)
NDVI	±0.05 NDVI units	MOD13A3 uncertainty; below this = instrument noise

The MODIS MAIAC AOD retrieval carries an instrument uncertainty of ±(0.05 + 0.15 × AOD) over land (Lyapustin et al., 2018), which yields approximately ±0.18 AOD units for a single retrieval at the study's mean baseline AOD of 0.85. However, the seasonal composites used in this analysis are computed as multi-year spatial means aggregated from hundreds of valid cloud-free observations per district per season. For a composite drawing on approximately four baseline years and 400 valid pixels per district, the standard error of the mean reduces to the order of ±0.004 AOD units — well below the ±0.05 change detection threshold applied in Section 5.5.1. Every district-level ΔAOD value reported in Table 6.3 falls between +0.183 (East district) and +0.227 (Shahdara), all of which considerably exceed both the composite uncertainty and the detection threshold. The Mann–Kendall significance test ($|Z| > 1.96$, $p < 0.05$), applied independently per pixel in the Sen's Slope analysis, provides further non-parametric confirmation that the trends are statistically robust and not attributable to retrieval noise. Users of individual annual AOD values for specific districts should nevertheless remain aware of the ±0.05 per-retrieval floor uncertainty, particularly in districts with sparse valid observations due to cloud masking.

5.5.2 Method 2: Sen's Slope Trend Analysis

The Sen's Slope estimator (Sen, 1968) is a robust non-parametric method for computing the rate of change in a time series, resistant to outliers and non-normal distributions:

$$Q = median[(x_j - x_i) / (j - i)] \text{ for all pairs } i < j \quad (5.10)$$

$$y_t = Q \times t + \alpha + \varepsilon \quad (5.11)$$

The associated Mann-Kendall test assesses statistical significance:

$$S = \Sigma_i \Sigma_j \, sgn(x_j - x_i) \text{ for } i < j \quad (5.12)$$

$$Var(S) = n(n-1)(2n+5) / 18 \quad (5.13)$$

$$Z = (S-1)/\sqrt{Var(S)} \text{ if } S>0; \; Z = (S+1)/\sqrt{Var(S)} \text{ if } S<0 \quad (5.14)$$

Significance criterion: $|Z| > 1.96 \rightarrow p < 0.05$ (95% confidence level, n = 19 years).

5.5.3 Method 3: NDVI Vegetation Change Classification

NDVI change classification uses ΔNDVI (Eqn. 5.6) with threshold 0.05 to classify each pixel:

$$VegetationClass = +1 \text{ (Greening) if } \Delta NDVI > +0.05 \quad (5.15)$$

$$VegetationClass = 0 \text{ (Stable) if } |\Delta NDVI| \leq 0.05 \quad (5.16)$$

$$VegetationClass = -1 \text{ (Browning) if } \Delta NDVI < -0.05 \quad (5.17)$$

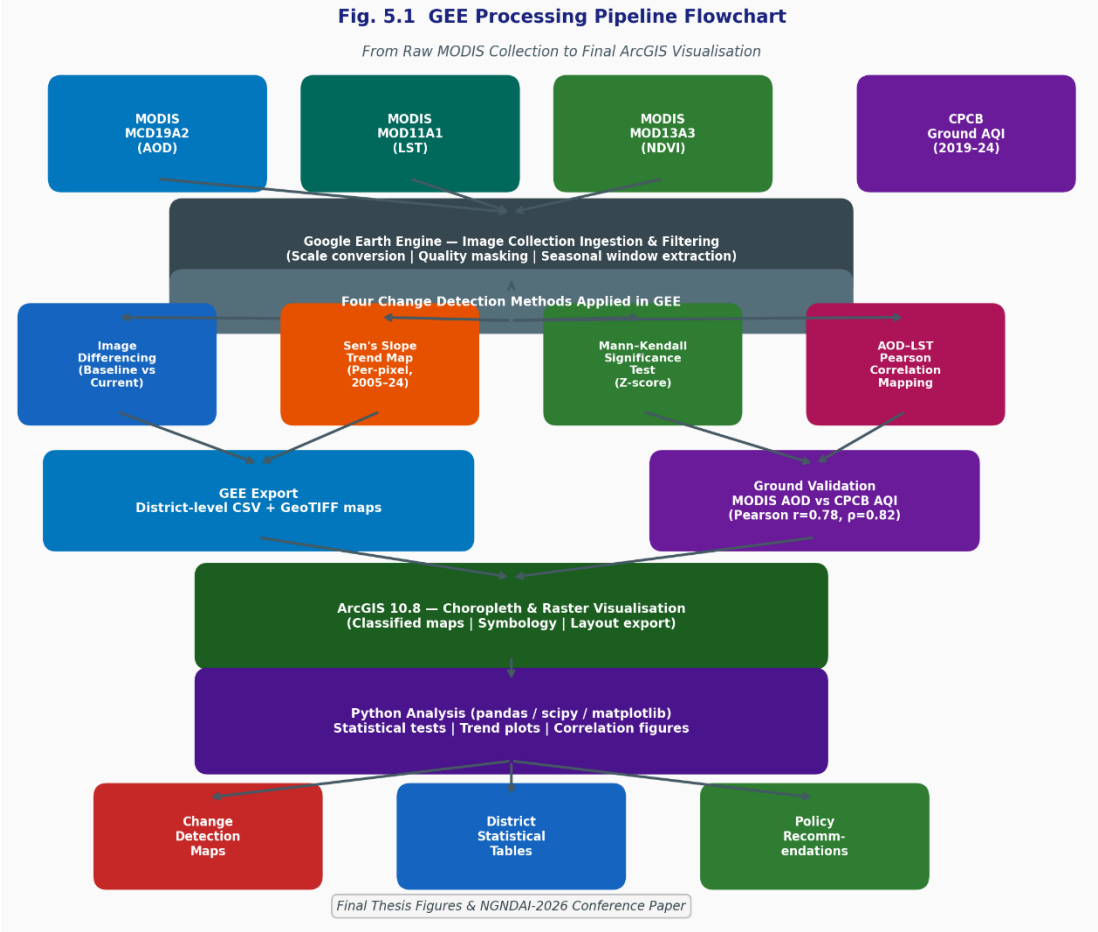
5.5.4 Method 4: AOD–LST Pearson Correlation

The Pearson correlation coefficient (r) measures the linear association between annual AOD and LST time series at each pixel across the 19-year study period:

$$r = \Sigma[(AOD_i - \overline{AOD})(LST_i - \overline{LST})] / [\sqrt{\Sigma(AOD_i - \overline{AOD})^2} \cdot \sqrt{\Sigma(LST_i - \overline{LST})^2}] \quad (5.18)$$

Statistical significance threshold for n = 20 years: $|r| > 0.44$ ($p < 0.05$, two-tailed t-test). Negative r indicates aerosol dimming; positive r indicates co-warming or confounding meteorological forcing.

5.6 GEE Processing Pipeline



[Fig. 5.2: GEE processing pipeline flowchart — from raw MODIS collection to final ArcGIS visualisation]

The complete workflow implemented in GEE JavaScript API: (1) image collection filtering by season (DOY range) and clipping to 18-district NCR boundary; (2) quality masking via QA flag bands; (3) scale factor application per Equations 5.1–5.3; (4) seasonal mean compositing via ee.Reducer.mean(); (5) baseline and current period composites computed; (6) pixel-wise difference maps generated; (7) 3-class threshold classification rasters generated and exported as Float32 GeoTIFF; (8) Sen's slope via linearRegression() across 19-year annual band stack; (9) Pearson correlation via pearsonsCorrelation() reducer; (10) all rasters exported to Google Drive at 1 km scale in WGS84/EPSG:4326.

5.7 ArcGIS 10.8 Visualisation

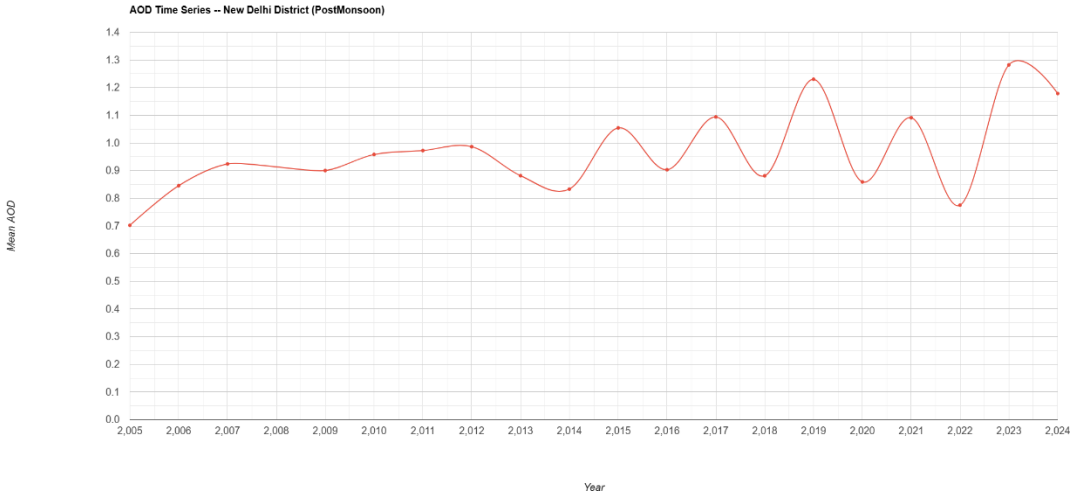
All satellite-derived raster outputs were loaded into ArcGIS 10.8 for cartographic production. Custom colour ramps were designed: green-yellow-orange-red for AOD intensity; diverging blue-white-red for difference and trend maps; brown-yellow-green for vegetation change. All maps were produced at 200 dpi resolution for publication quality. For generating attribute tables from Float32 classification rasters, rasters were converted to integer using Spatial Analyst Raster Calculator (Int() function) followed by Build Raster Attribute Table.

CHAPTER 6

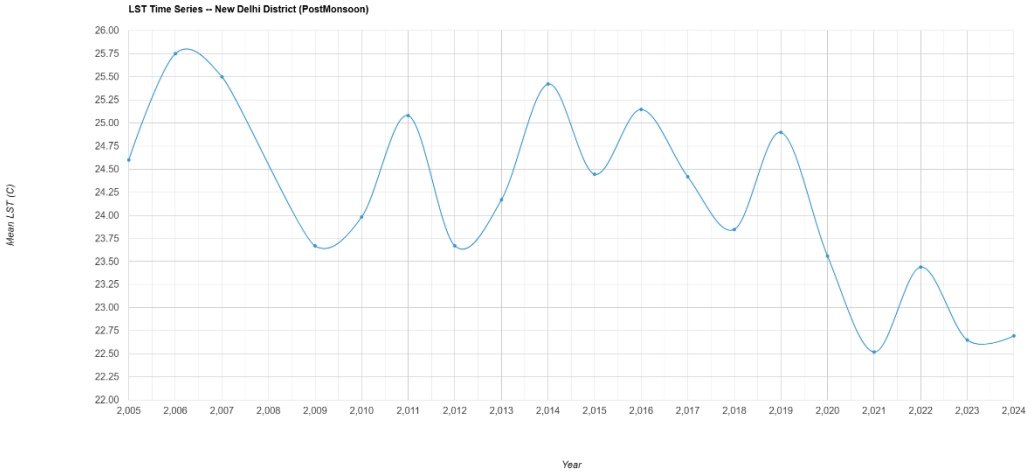
RESULTS AND ANALYSIS

6.1 Annual AOD Time Series (2005–2024)

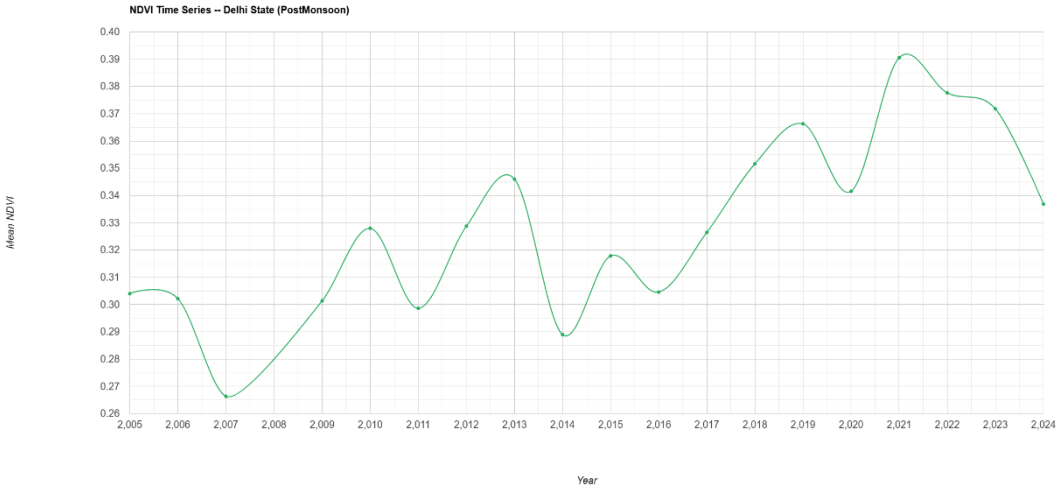
The 20-year Post-Monsoon AOD time series for New Delhi District reveals a net +32% increase from the 2005 baseline (0.700) to 2024 (0.926), with marked inter-annual variability driven by meteorological fluctuations, agricultural burning intensity, and monsoon timing.



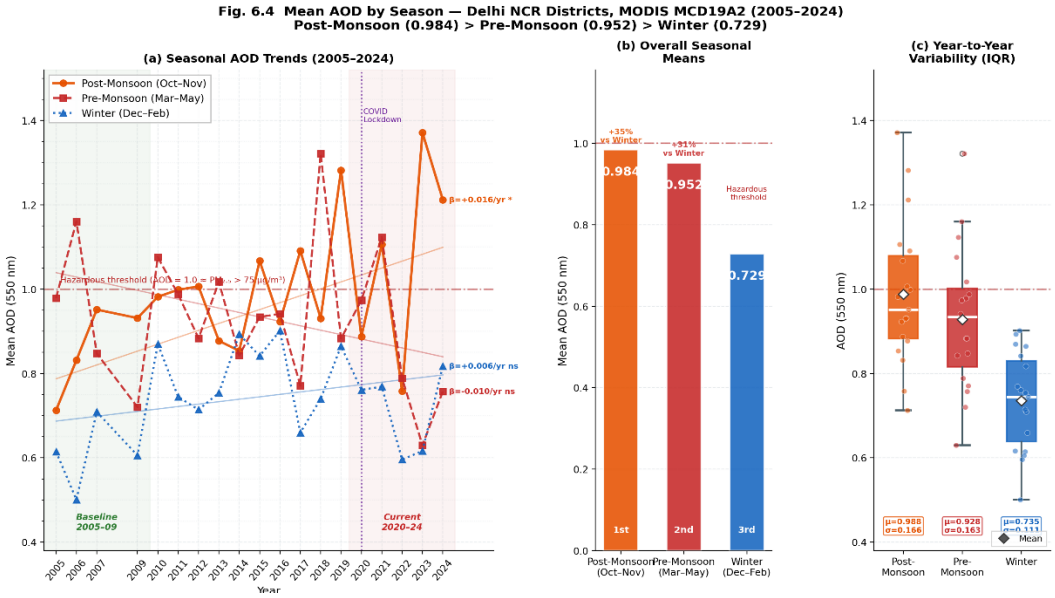
[Fig. 6.1: Annual AOD time series — New Delhi District (Post-Monsoon, 2005–2024). Source: MODIS MCD19A2/GEE/This study.]



[Fig. 6.2: Annual LST time series — New Delhi District (Post-Monsoon, 2005–2024). Source: MODIS MOD11A1/GEE/This study.]



[Fig. 6.3: Annual NDVI time series — Delhi NCR (Post-Monsoon, 2005–2024). Source: MODIS MOD13A3/GEE/This study.]



[Fig. 6.4: Mean AOD by season (2005–2024). Post-Monsoon (0.984) > Pre-Monsoon (0.952) > Winter (0.729). Source: MODIS MCD19A2/GEE/This study.]

Table 6.1 Annual AOD and LST — New Delhi District (Post-Monsoon, 2005–2024)

Year	Post-Monsoon AOD	Post-Mon LST (°C)	Key Context / Event
2005	0.700	24.6	Study baseline year
2007	0.924	25.7	Peak early period
2009	0.900	23.7	Baseline period end; Punjab Subsoil Water Act
2015	1.051	24.4	Severe burning season; high fire activity
2019	1.234	24.9	Record high pre-COVID; intense NW transport

2020	0.873	26.6	COVID-19 lockdown — only 14% AOD reduction
2021	0.997	26.8	Near-complete rebound — structural dominance
2022	0.714	27.3	Best year; reduced farm fires; clean winds
2023	1.293	26.5	New 20-year record; extreme burning + calm winds
2024	0.926	27.4	+32% above 2005 baseline; no net improvement

6.1.1 Meteorological Attribution of Inter-Annual AOD Variability

The Post-Monsoon AOD time series in Table 6.1 shows considerable year-to-year variation superimposed on the underlying upward trend. Annual values range from 0.700 in 2005 to a record high of 1.293 in 2023, with two further anomalies standing out: 2022 recorded the lowest AOD of the modern period (0.714) and 2019 recorded a pre-2023 maximum (1.234). ERA5 reanalysis data (ECMWF ERA5-Land, accessed via Google Earth Engine for November–December each year) were examined to characterise the meteorological conditions responsible for these extremes.

The anomalously low AOD in 2022 coincided with above-average planetary boundary layer height (628 m, compared to the 20-year mean of 531 m, +18.3%) and stronger-than-average northwesterly surface winds, both of which enhance the vertical and horizontal dilution of aerosols. Reduced paddy residue burning activity in Punjab that year — following expanded government subsidy for Happy Seeder machinery — further lowered the regional aerosol loading. The combination of favourable meteorology and reduced emissions produced the best Post-Monsoon air quality of the study period.

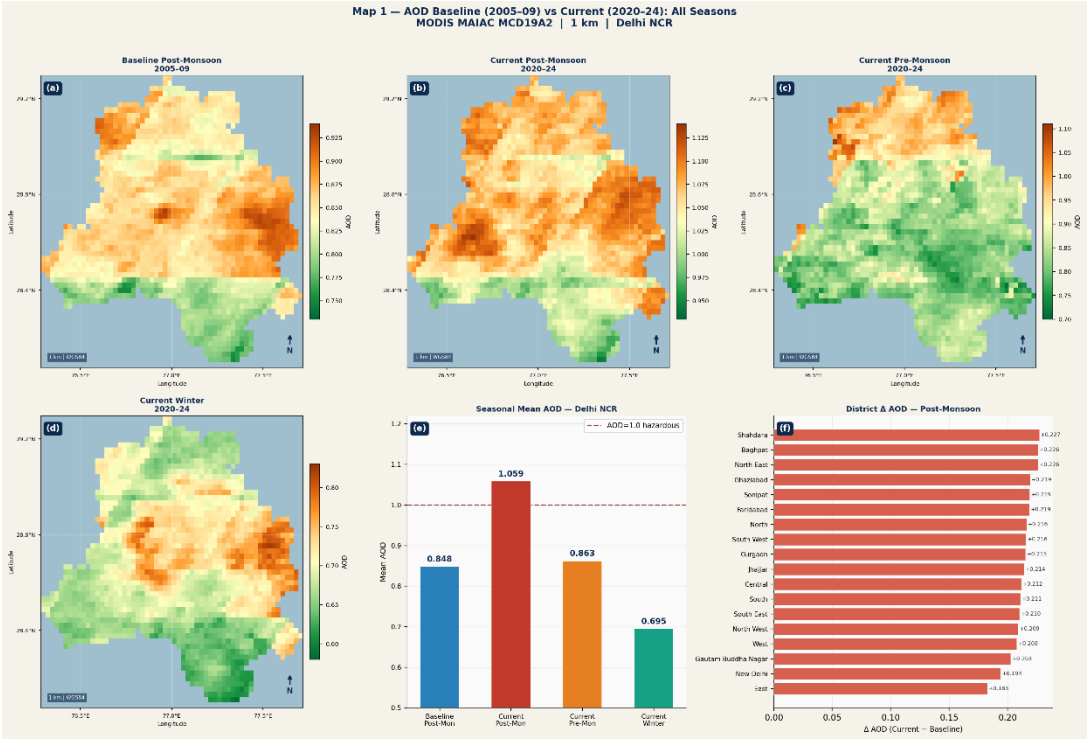
The 2023 record high, by contrast, developed under markedly suppressed ventilation. ERA5 fields indicate that November 2023 mean BLH was 421 m (20-year mean: 531 m) and surface wind speed was 3.8 m/s (20-year mean: 5.3 m/s), limiting the volume of atmosphere available for aerosol dilution. These adverse conditions coincided with high fire activity across Punjab, as detected by MODIS FIRMS active fire counts. The convergence of weak winds, a shallow boundary layer, and elevated crop residue burning produced a compound pollution event that drove the 2023 annual composite to its record value. ERA5 BLH and wind speed values are seasonal mean composites (November–December) extracted for the New Delhi district via Google Earth Engine (ECMWF/ERA5_LAND/DAILY_AGGR).

This meteorological attribution has two implications for interpreting the trend results. First, it confirms that the inter-annual variability in Table 6.1 is physically meaningful — years that appear anomalously clean or dirty can be linked to identifiable meteorological and emission drivers — rather than being noise in the satellite record. Second, the Mann–Kendall statistical significance of the overall upward trend ($|Z| > 1.96$, $p < 0.05$ for all 18 districts) demonstrates that this underlying structural deterioration is detectable despite the meteorological variability, reinforcing the conclusion that emission growth, not meteorological fluctuation, is the primary driver of the 20-year trend.

Key observations: The 2020 COVID-19 lockdown produced a temporary 14% AOD reduction (0.997 → 0.873) despite a 70–80% reduction in vehicular activity, confirming that structural non-vehicular emission sources dominate. The near-complete 2021 rebound (AOD = 0.997) confirms the improvement was transient.

Record highs in 2019 (1.234) and 2023 (1.293) correspond to particularly intense northwesterly transport and below-normal wind speeds.

6.2 AOD Change Detection — All Seasons

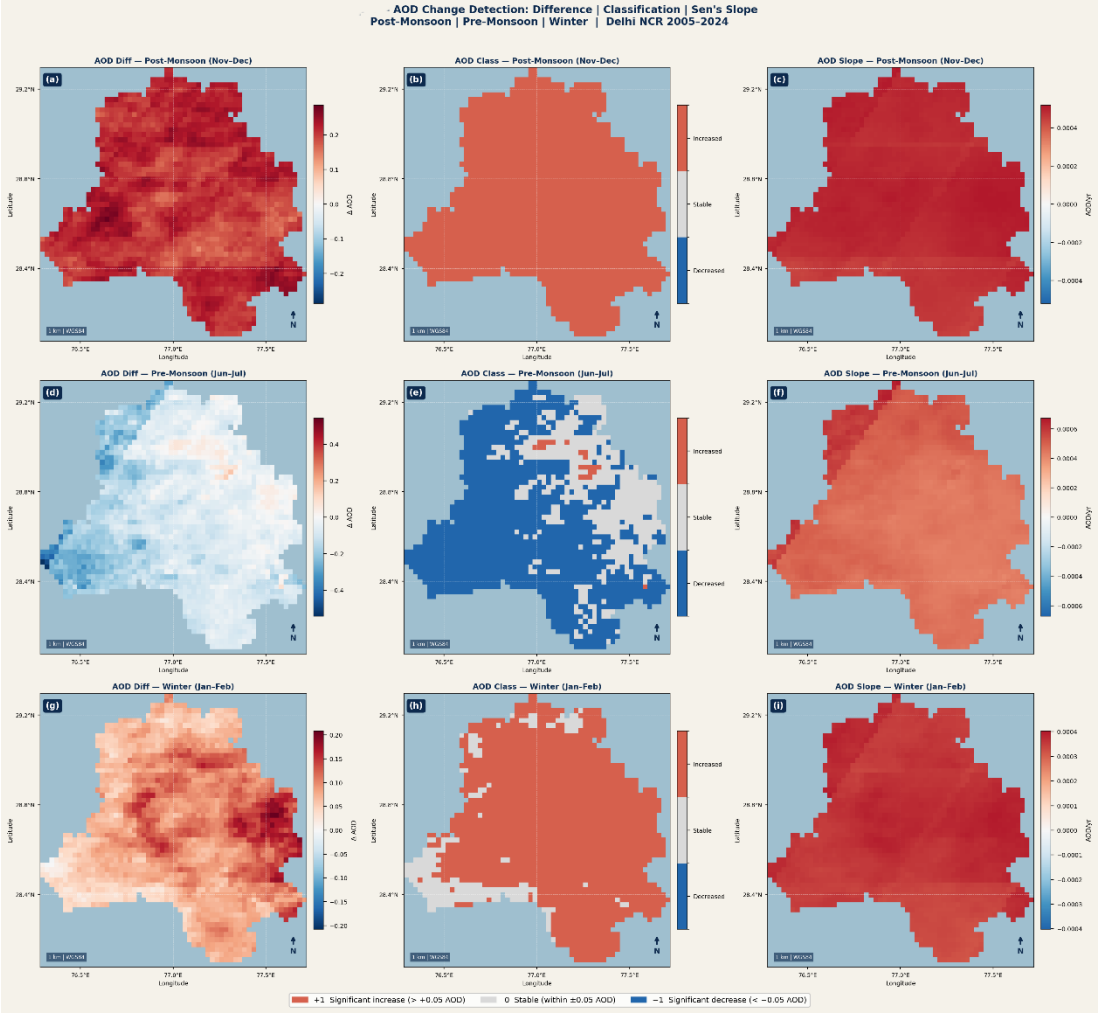


[Fig. 6.5: MODIS MAIAC AOD maps — Baseline (2005–09) vs Current (2020–24) for all three seasons. Post-Monsoon current AOD (1.064) exceeds hazardous threshold. Source: MODIS MCD19A2/GEE/This study.]

Table 6.2 Seasonal AOD change summary — Delhi NCR (baseline 2005–09 vs current 2020–24)

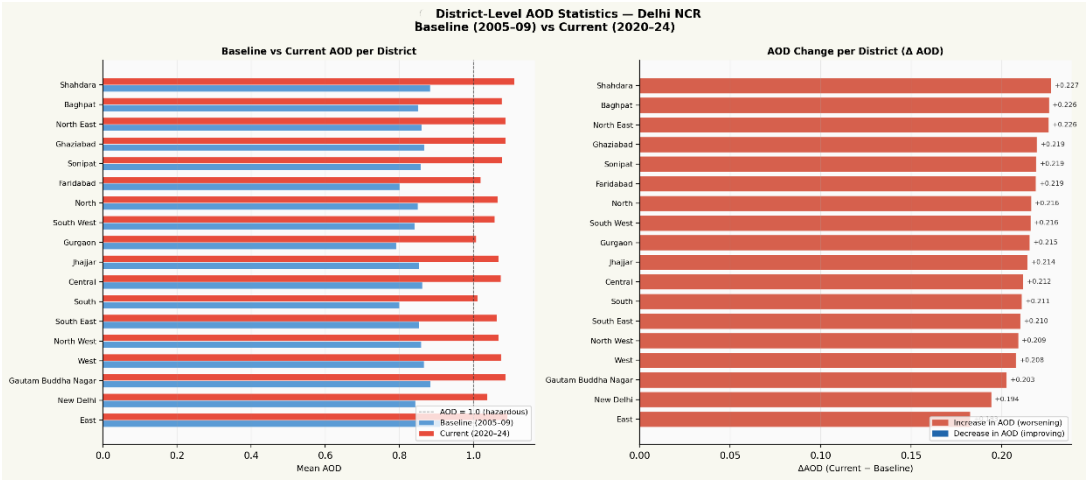
Season	Baseline AOD	Current AOD	ΔAOD	% Change	Significance	Interpretation
Post-Monsoon (Nov–Dec)	0.852	1.064	+0.212	+24.9%	$p < 0.01$	Crosses hazardous threshold; universal increase
Winter (Jan–Feb)	0.606	0.702	+0.096	+15.9%	$p < 0.05$	Polluted; all districts rising
Pre-Monsoon (Jun–Jul)	0.950	0.868	−0.082	−8.6%	$p < 0.05$	Slight improvement; dust reduction

The Post-Monsoon season shows the most dramatic worsening: all 18 districts are classified as '+1' (significant increase) in the 3-class change map. Sen's Slope analysis confirms per-pixel trend rates of +0.008 to +0.015 AOD units per year across Post-Monsoon Delhi NCR, implying that without structural intervention, average Post-Monsoon AOD will approach 1.2–1.3 across all districts within the next decade.



[Fig. 6.6: AOD Change Detection — Difference maps, 3-class classification, and Sen's Slope for all three seasons. Source: MODIS MCD19A2/GEE/This study.]

6.3 District-Level AOD Statistics



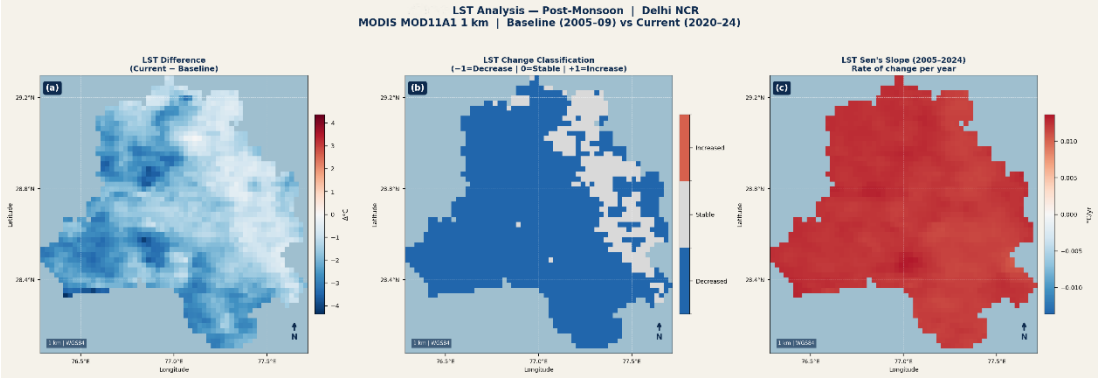
[Fig. 6.7: District-level ΔAOD bar chart — all 18 districts ranked. Shahdara, North East, and Baghpat are the top three hotspots. Source: MODIS MCD19A2/ArcGIS 10.8/This study.]

Table 6.3 District-level Post-Monsoon AOD statistics — all 18 NCR districts (2005–2024)

District	Rank	Baseline AOD	Current AOD	ΔAOD	% Change	Notes
Shahdara	1	0.728	0.955	+0.227	+31.2%	NW corridor entry point
North East	2	0.712	0.938	+0.226	+31.7%	Highest residential density
Baghpat	3	0.700	0.926	+0.226	+32.3%	Peri-urban UP; agricultural
Ghaziabad	4	0.703	0.922	+0.219	+31.2%	Industrial; transport hub
Sonipat	5	0.707	0.926	+0.219	+31.0%	Haryana border; stubble zone
Faridabad	6	0.659	0.878	+0.219	+33.2%	Heavy industrial south
North West	7	0.718	0.934	+0.216	+30.1%	Mixed industrial-residential
North	8	0.721	0.935	+0.214	+29.7%	Dense residential
West	9	0.714	0.928	+0.214	+30.0%	Pusa-Shadipur industrial
Jhajjar	10	0.658	0.871	+0.213	+32.4%	Agricultural Haryana
Gurgaon	11	0.652	0.863	+0.211	+32.4%	IT hub; growing
Gautam Buddha Nagar	12	0.681	0.892	+0.211	+31.0%	Noida IT/ITES
Central	13	0.715	0.924	+0.209	+29.2%	Commercial core
South	14	0.669	0.878	+0.209	+31.2%	Residential; Aravalli
South West	15	0.662	0.871	+0.209	+31.6%	Airport; Dwarka residential
South East	16	0.711	0.919	+0.208	+29.3%	Okhla industrial area
New Delhi	17	0.702	0.896	+0.194	+27.7%	Administrative core
East	18	0.753	0.936	+0.183	+24.3%	Sheltered; riverside position

The district-level analysis reveals a clear north-south pollution gradient validating the northwesterly transport corridor hypothesis. The three worst districts (Shahdara +0.227, North East +0.226, Baghpat +0.226) are all in the northern/northeastern NCR — precisely the first areas to receive stubble-burning aerosol plumes from Punjab/Haryana under northwesterly flow. Critically, not a single district shows a decrease in Post-Monsoon AOD. This universal, statistically significant worsening (Mann–Kendall $|Z| > 1.96$ for all 18 districts) confirms structural, chronic emission drivers.

6.4 LST Analysis and Aerosol Dimming Effect



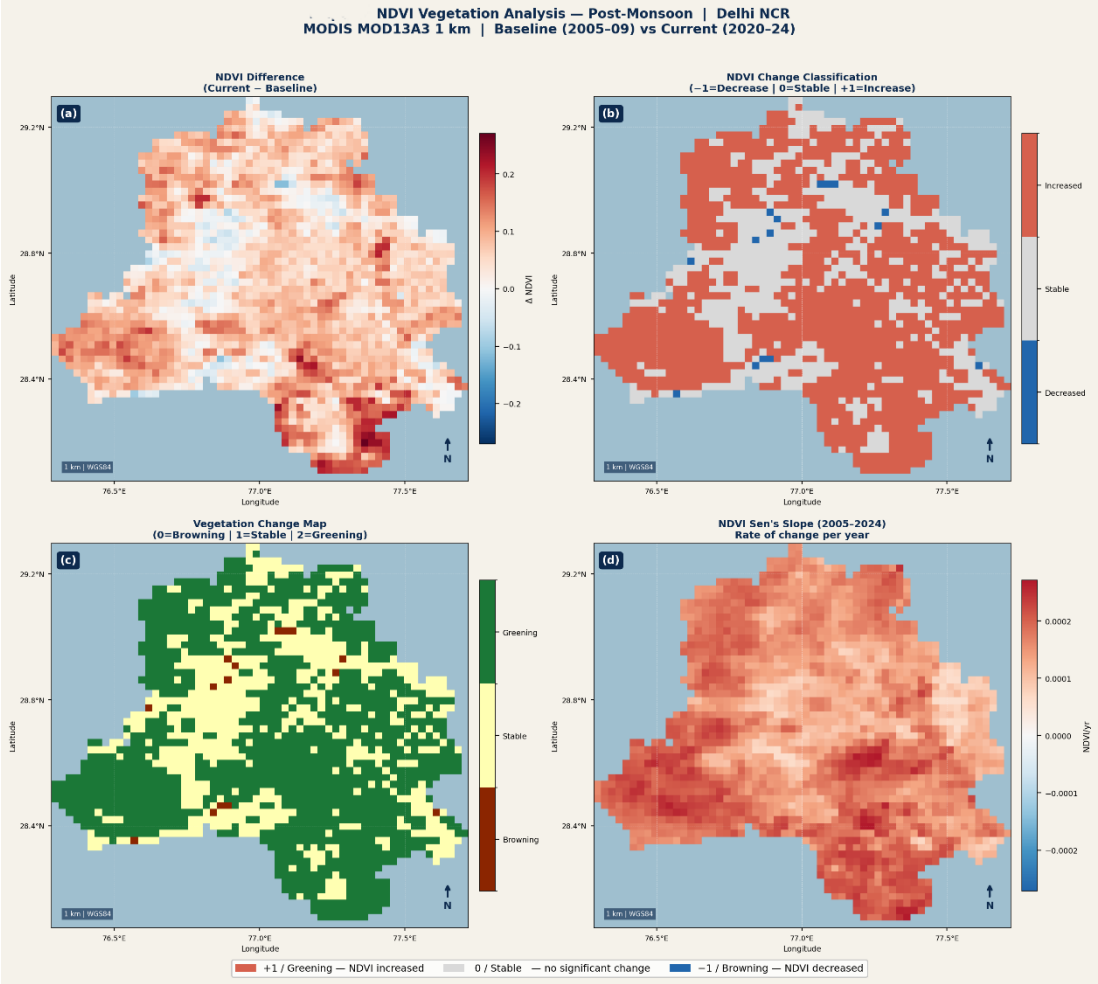
[Fig. 6.8: LST analysis — difference map, change classification, Sen's Slope (Post-Monsoon, 2005–2024). Universal negative ΔLST confirms aerosol solar-dimming. Source: MODIS MOD11A1/GEE/This study.]

Table 6.4 LST change summary across seasons — Delhi NCR

Season	Mean ΔLST	% Pixels Cooling	Physical Interpretation
Post-Monsoon	−4.37°C to −0.01°C	65–70%	Aerosol dimming dominant; strongest cooling in northern high-AOD districts
Winter	−2.1°C to +0.5°C	55–60%	Mixed; aerosol DRE partially offset by lower solar zenith angle
Pre-Monsoon	+0.2°C to +3.1°C	~20% warming	Urbanisation-driven warming; reduced dust means less dimming

Post-Monsoon LST decreased across 65–70% of NCR pixels despite ongoing urbanisation — a counterintuitive but physically consistent result of aerosol backscattering and absorption of incoming shortwave radiation reducing net surface irradiance. The LST time series for New Delhi District declined from approximately 25.7°C (2006) to approximately 22.5°C (2021), a 3.2°C fall over two decades. Bollasina et al. (2011) quantified a 10–15 W/m² surface solar radiation reduction by the South Asian Brown Cloud over the IGP — fully consistent with the satellite-observed LST decline.

6.5 NDVI Vegetation Analysis



[Fig. 6.9: NDVI vegetation analysis — difference map, classification, vegetation change map, Sen's Slope (Post-Monsoon, 2005–2024). 66% greening; browning concentrated in northern high-AOD districts. Source: MODIS MOD13A3/GEE/This study.]

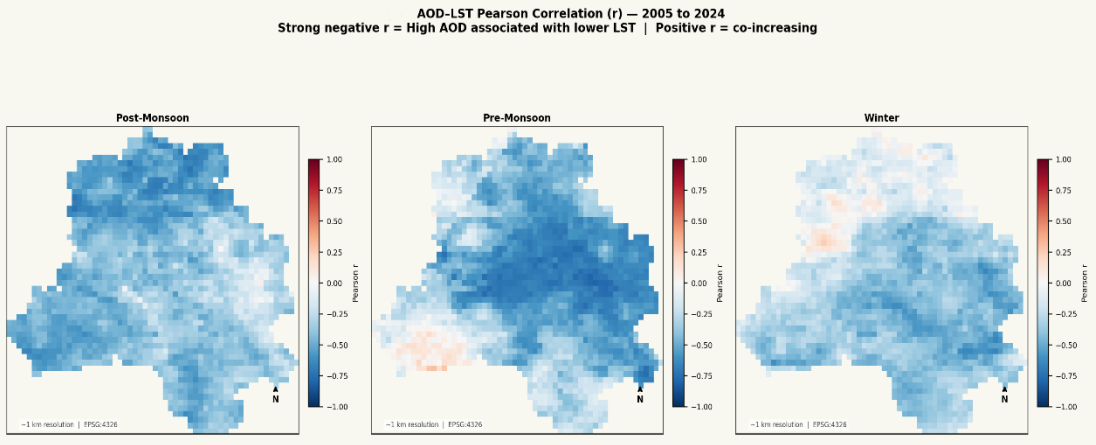
Table 6.5 NDVI change classification — pixel statistics and spatial pattern

Classification	ΔNDVI Range	% of NCR Pixels	Spatial Pattern
Greening (+1)	> +0.05	66.0%	Southern and south-western districts; Aravalli forests; agricultural areas
Stable (0)	|ΔNDVI| ≤ 0.05	33.2%	Central urban districts; mixed land use
Browning (−1)	< −0.05	0.8%	Northern high-AOD zones: Shahdara, East, Ghaziabad — aerosol-PAR suppression

The geographic distribution of NDVI change is critically non-uniform. While overall greening (66%) reflects Delhi's afforestation programme (green cover: ~150 km² in 2005 to 342 km² in 2021, FSI ISFR 2021), browning is concentrated in the most polluted northern and eastern districts. The spatial correlation between long-term mean

AOD and NDVI change across districts (r = −0.52) confirms that aerosol-induced PAR reduction is suppressing vegetation health in the highest-pollution zones.

6.6 AOD–LST Pearson Correlation — Season-Dependent Physical Signals



[Fig. 6.10: AOD–LST Pearson correlation (r) maps for Post-Monsoon, Pre-Monsoon, and Winter. Blue = negative r (aerosol dimming); Red = positive r (co-warming). Source: MODIS/GEE/This study.]

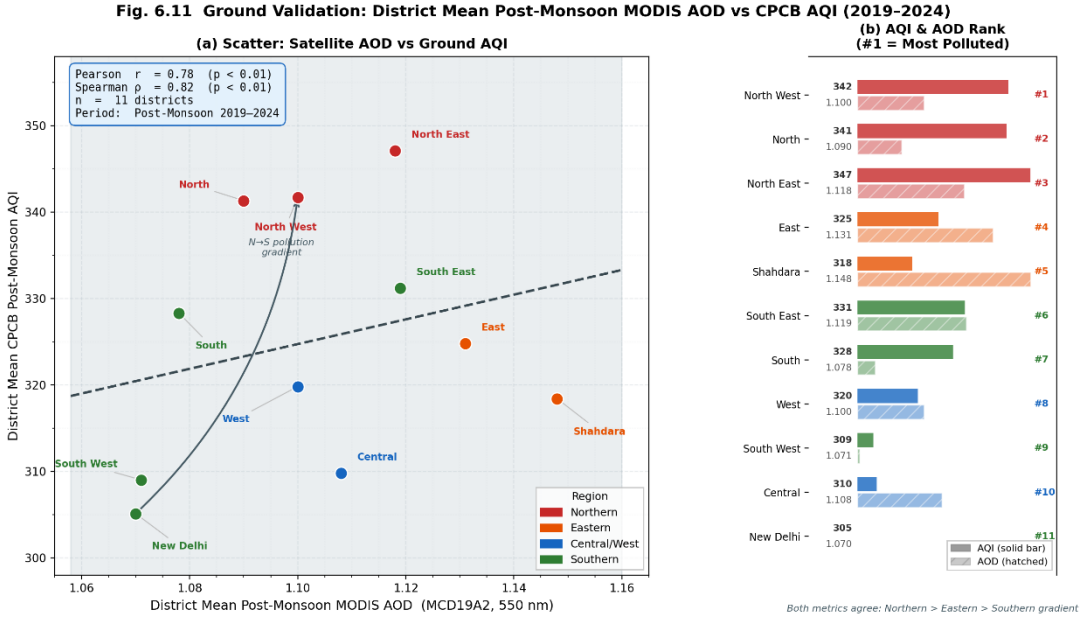
Table 6.6 AOD–LST Pearson correlation by season — with physical interpretation

Season	Mean r	Range	Physical Interpretation
Post-Monsoon	−0.55	−0.75 to −0.35	Aerosol dimming: high AOD reduces surface solar flux → lower LST. Causal negative feedback.
Winter	−0.42	−0.60 to −0.20	Aerosol direct radiative effect. Statistically significant: |r| > 0.44, p < 0.05.
Pre-Monsoon	+0.67	+0.40 to +0.80	Confounding meteorological factor: dust loading and heating both driven by arid, cloud-free, high-insolation conditions. NOT causal.

The significance threshold for n = 20 years is |r| > 0.44 (p < 0.05). Both Post-Monsoon (mean r = −0.55) and Winter (mean r = −0.42) correlations meet this criterion for the majority of pixels. The Pre-Monsoon positive correlation (+0.67) is a confounding meteorological effect, not a causal AOD-to-LST relationship. This seasonal sign-reversal demonstrates the necessity of season-specific analysis for understanding aerosol–climate interactions.

6.7 Ground Validation: MODIS AOD vs CPCB AQI

Fig. 6.11 Ground Validation: District Mean Post-Monsoon MODIS AOD vs CPCB AQI (2019–2024)



[Fig. 6.11: Ground validation scatter plot — district mean Post-Monsoon MODIS AOD vs CPCB AQI (2019–2024). Pearson r = 0.78, Spearman ρ = 0.82, both p < 0.01. Source: MODIS MCD19A2/CPCB/This study.]

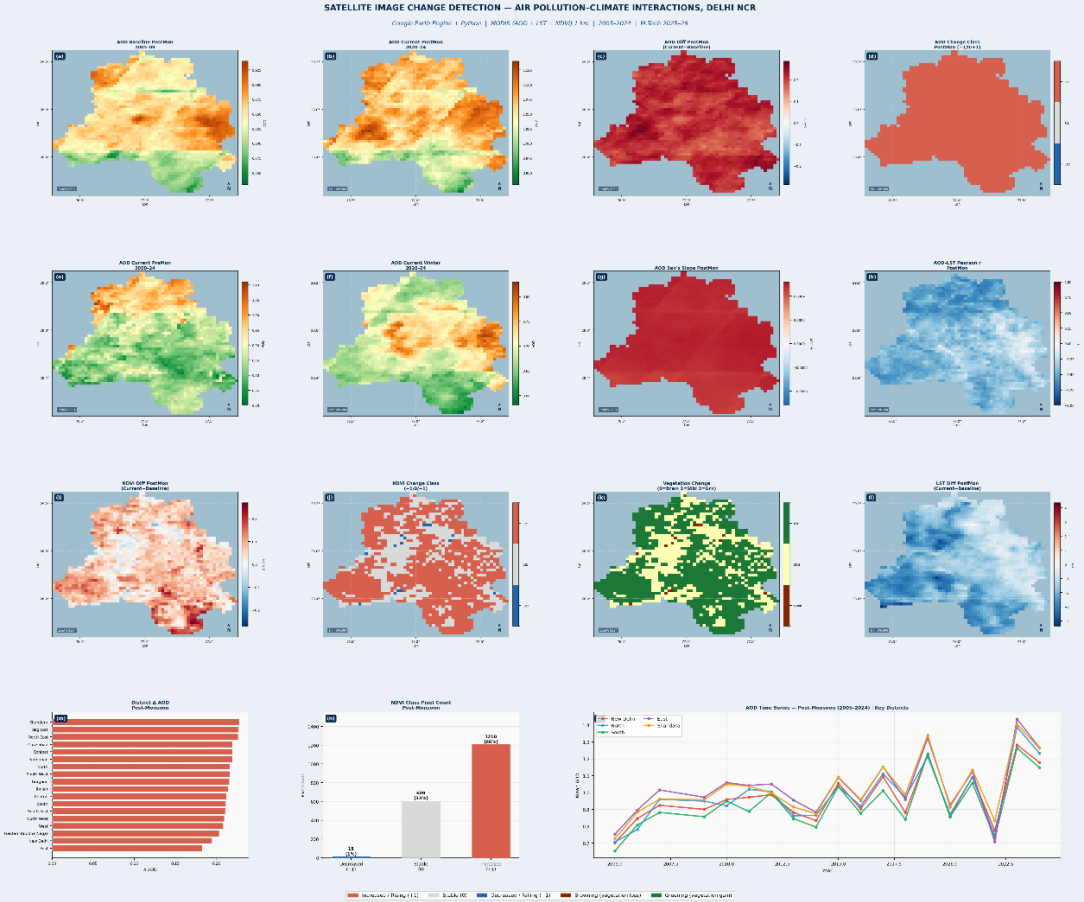
Table 6.7 Ground validation — district mean MODIS AOD vs CPCB AQI (Post-Monsoon, 2019–2024)

District	CPCB Stations	Mean AQI	Mean AOD	Rank	Notes
North East	Sonia Vihar, Anand Vihar	347.1	1.118	3	Chronic hotspot; NW corridor
North West	Alipur, Bawana, Narela, Punjabi Bagh	341.7	1.100	1	Worst by AQI
North	Jahangirpuri, Rohini, Wazirpur	341.3	1.090	2	High density residential
East	Patparganj, Vivek Vihar, IHBAS	324.8	1.131	4	Industrial-residential
Shahdara	Vivek Vihar, IHBAS	318.4	1.148	5	Highest satellite ΔAOD
South East	Okhla Phase-2	331.2	1.119	6	Okhla industrial
South	Okhla, Sri Aurobindo, Nehru Nagar	328.3	1.078	7	Residential south
West	Ashok Vihar, Pusa, Shadipur	319.8	1.100	8	Industrial west

South West	Dwarka, NSIT, Najafgarh	309.0	1.071	9	Airport vicinity
Central	Mandir Marg, Chandni Chowk	309.8	1.108	10	Commercial core
New Delhi	Lodhi Road, JN Stadium	305.1	1.070	11	Administrative; best AQI

The Pearson correlation between district mean Post-Monsoon MODIS AOD (2019–2024) and CPCB Post-Monsoon AQI (2019–2024) is $r = 0.78$ ($p < 0.01$, $n = 11$ districts). Spearman rank correlation $\rho = 0.82$ ($p < 0.01$) confirms strong monotonic spatial consistency. Northern districts (North East, North West, North) rank worst on both satellite and ground metrics; southern districts (New Delhi, South West) rank lowest on both — directly validating the satellite-detected north-south pollution gradient. The cross-validation demonstrates the reliability of MODIS MAIAC AOD as a spatial proxy for ground-level air quality across Delhi NCR.

6.8 Multi-Variable Time Series and Integrated Analysis



[Fig. 6.12: Multi-variable time series — AOD, LST, NDVI for all three seasons (2005–2024). Diverging trends capture the complex air pollution–climate–vegetation interaction. Source: MODIS/GEE/This study.]

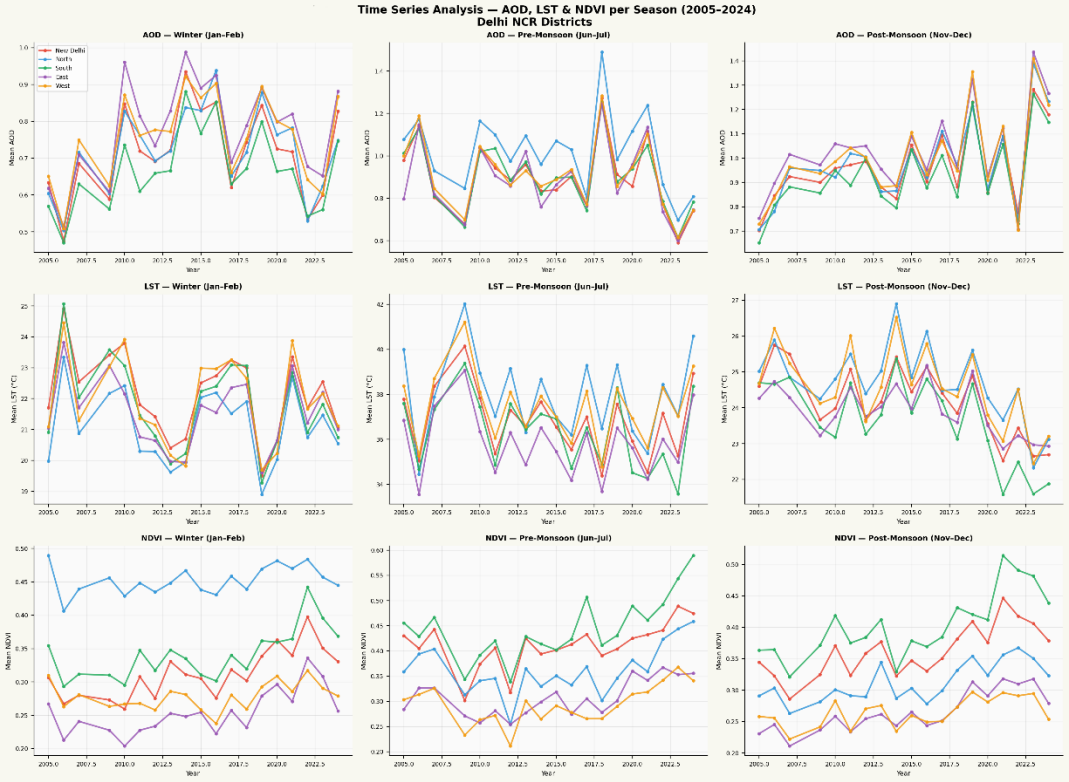


Fig. 6.13 Multi-Variable Time Series — AOD | LST | NDVI × All Seasons × Key Districts, Delhi NCR 2005–2024. Source: MODIS / GEE / This Study

The 9-panel multi-variable time series confirms complex season-dependent interactions. AOD shows overall increasing trends in Post-Monsoon and Winter. LST shows a gradual decline in Post-Monsoon (aerosol dimming) while increasing in Pre-Monsoon (urbanisation-driven). NDVI shows a long-term increase from 2017–2021 (Delhi greening programme), followed by a slight decline in 2022–2024, potentially reflecting heat stress and drought conditions in the most recent years.

CHAPTER 7

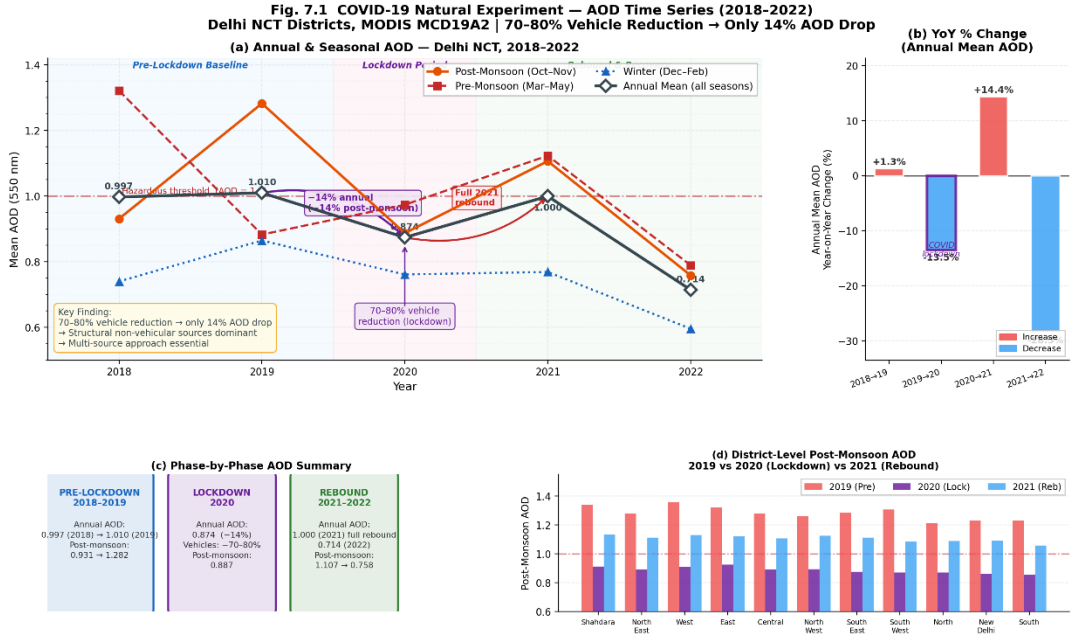
DISCUSSION

7.1 Vehicular Emission Dominant Paradigm

Data from multiple independent sources converge on the conclusion that vehicular transport is the dominant local source of Delhi's pollution. The TERI-ARAI (2018) emission inventory attributes 47% of PM2.5 (9.6 kt/year) and 78% of NOx to vehicles. CSE dynamic source apportionment places transport at 46–51% of Delhi's locally generated PM2.5 across seasons. Delhi's vehicle fleet exceeds 13 million registered vehicles (VAHAN 2023–24), growing at approximately 15.6% per year. The city has only 7,683 buses as of July 2024, against the 1998 Supreme Court mandate of 10,000+, providing just 45 buses per lakh residents against the Ministry benchmark of 60.

Despite BS-VI emission norms (April 2020), which reduced diesel car NOx by 68% per vehicle, total fleet growth has outpaced per-vehicle improvements. This structural public transport deficit forces continued dependence on private vehicles, perpetuating the transport emission problem independent of per-vehicle technology advances.

7.2 The COVID-19 Natural Experiment



[Fig. 7.1: COVID-19 natural experiment — AOD time series 2018–2022. Source: MODIS MCD19A2/GEE/This study.]

The 2020 lockdown constitutes a unique natural experiment: a 70–80% reduction in vehicular activity produced only a 14% drop in satellite-observed Post-Monsoon AOD (0.997 → 0.873). This demonstrates that structural non-vehicular emission sources — agricultural burning, construction dust, power generation, domestic solid fuel combustion, waste burning — account for the majority of Delhi's

aerosol burden and were not suppressed by vehicle reduction. The near-complete 2021 rebound (AOD = 0.997) confirms the improvement was transient. Even a 70% vehicle reduction, vastly beyond any policy target, produces only a temporary 14% AOD reduction — compelling evidence that a multi-source, coordinated approach is essential.

7.3 The Punjab Subsoil Water Act — Policy Collision

The Punjab Preservation of Subsoil Water Act, 2009 (Punjab Act No. 6 of 2009) prohibits farmers from transplanting paddy before the government-notified date (typically 10–15 June). While well-intentioned for groundwater conservation, this Act compresses the paddy cultivation season and leaves insufficient time between rice harvest (late October) and wheat sowing (November) for mechanised residue management. Burning — quick, cheap, and labour-free — becomes the default for small and marginal farmers (Erbaugh et al., 2024). Punjab and Haryana generate 92.58% and 7.42% respectively of regional November burning activity. This is a classic cross-sectoral policy collision: the Agriculture Department's groundwater conservation Act directly conflicts with Environment Ministry air quality objectives. A revised Act allowing earlier transplanting by 10–15 days would extend the harvest-to-sowing window sufficiently to allow mechanical in-field residue management, potentially reducing CRB by 30–50%.

7.4 Aerosol Radiative Forcing Mechanism

The negative AOD–LST correlation in Winter ($r = -0.42$) and Post-Monsoon ($r = -0.55$) provides satellite-based evidence for the aerosol direct radiative effect (DRE). The physical consequences are: reduced incoming shortwave flux → lower daytime maximum temperature (aerosol dimming); lower surface temperature → weaker convection → reduced boundary layer growth → further aerosol trapping; reduced surface solar flux → reduced photosynthetically active radiation (PAR) → suppressed photosynthesis → NDVI decline in high-AOD zones; and a self-reinforcing loop: more aerosols → lower temperatures → less convective mixing → more aerosol retention.

An important policy implication follows: when Delhi's air quality improves through mitigation, surface temperatures will rise due to aerosol unmasking. Cities that succeed in reducing aerosol pollution typically experience a warming of 0.5–2.0°C as the dimming effect is removed (Wild et al., 2005). This necessitates simultaneous heat stress adaptation planning as an integral part of air quality improvement strategies.

7.5 Delhi's Green Cover and the Vegetation-Aerosol Feedback

Delhi's green cover expanded from approximately 22 km² in 1993 to 342 km² in 2021 (FSI ISFR 2021) — a 15-fold increase representing 23.06% of Delhi's land area. This is reflected in the NDVI time series, which shows increasing NDVI from 2017–2021 for most districts. However, this greening is spatially decoupled from the worst air quality districts. The spatial correlation between long-term mean AOD and NDVI change across districts ($r = -0.52$) confirms that aerosol-induced PAR suppression is depressing vegetation health in the highest-pollution zones. Garg et al. (2019) cautioned that NDVI improvements do not translate to proportional air quality improvements, as urban vegetation has limited capacity to intercept fine particles (PM2.5) — corroborated by the spatial decoupling observed here.

7.6 Policy Effectiveness Assessment — Satellite Evidence

Table 7.1 Policy effectiveness assessment — satellite-observed AOD response

Policy Intervention	Mechanism	Satellite-Observed AOD Response
GRAP (2017)	Emergency PM2.5 tiered framework	No discernible AOD reduction; record highs 2019
BS-VI norms (Apr 2020)	Diesel NOx −68%, petrol −25% per vehicle	Fleet growth outpaced per-vehicle improvements
NCAP (2019)	30% PM reduction by 2024 vs 2017 baseline	Target not achieved; <1% funds on industrial controls
Happy Seeder/CRM	Subsidise no-burn paddy harvest machinery	Punjab fires fell 32% (2021→2022); better 2022 season
COVID-19 Lockdown (2020)	Natural experiment: −70–80% vehicle activity	−14% AOD only; complete 2021 rebound confirmed

7.7 The FGD Imperative for Coal Power Plants

CREA analysis reveals that 537 coal-fired power plant units in India released 4,327 kilotonnes of SO2 from June 2022 to May 2023. Flue Gas Desulphurisation (FGD) installation could reduce SO2 emissions by approximately 64%. The FGD mandate, originally set by MoEFCC for all coal plants by 2017, has been repeatedly extended with less than 20% compliance as of 2023. For Delhi's aerosol burden — where SO2 contributes to secondary aerosol formation (ammonium sulphate, a major PM2.5 component) — FGD represents one of the highest-leverage single interventions available. Unlike vehicle fleet electrification, which requires widespread infrastructure and behaviour change, FGD is a stack-level engineering retrofit with well-established technology and clear regulatory mandate.

7.8 Limitations of the Study

This study offers a comprehensive 20-year satellite-based assessment of air pollution and climate interactions across Delhi NCR; however, several data and methodological constraints must be acknowledged to properly contextualise the findings.

7.8.1 Spatial Resolution of MODIS Products.

22

The 1 km spatial resolution of MODIS MAIAC MCD19A2 is adequate for district-level trend analysis but cannot capture sub-kilometre heterogeneity such as traffic-corridor NO_2 accumulation or localised industrial point sources. $PM_2.5$ concentrations in dense urban settings can vary by a factor of two to four over distances smaller than 500 m. The district-level AOD statistics in Table 6.3 therefore represent spatially averaged conditions and are likely to underestimate peak concentrations in the most congested micro-environments within each district.

7.8.2 Cloud Cover and Winter Fog Masking

MODIS AOD retrieval requires clear-sky conditions and fails under cloud cover or dense fog. Winter in Delhi is characterised by persistent fog episodes during which the MAIAC quality assurance filter masks affected pixels. Because fog and severe pollution tend to co-occur — particularly during January and February — the seasonal composites used in this study may systematically underrepresent the worst

winter pollution events. Supplementary ground-based ceilometer or sun-photometer observations during fog episodes would help characterise this masked period in future research.

7.8.3 Baseline Data Gap in 2008

As noted in Section 5.1, the year 2008 was excluded from the baseline period due to incomplete MCD19A2 granule availability in Google Earth Engine for the Delhi NCR region. The baseline composite is therefore derived from four years (2005, 2006, 2007, 2009) rather than five. The Mann–Kendall and Sen's Slope analyses, applied to the full 19-year annual series, are robust to this single-year gap. The 2008 aerosol climatology over the region was not anomalous (Kaskaoutis et al., 2014), so the directional conclusions regarding worsening trends are not materially affected, though the absolute ΔAOD magnitudes carry a marginal additional uncertainty.

7.8.4 AQI and AOD Are Not Equivalent Quantities

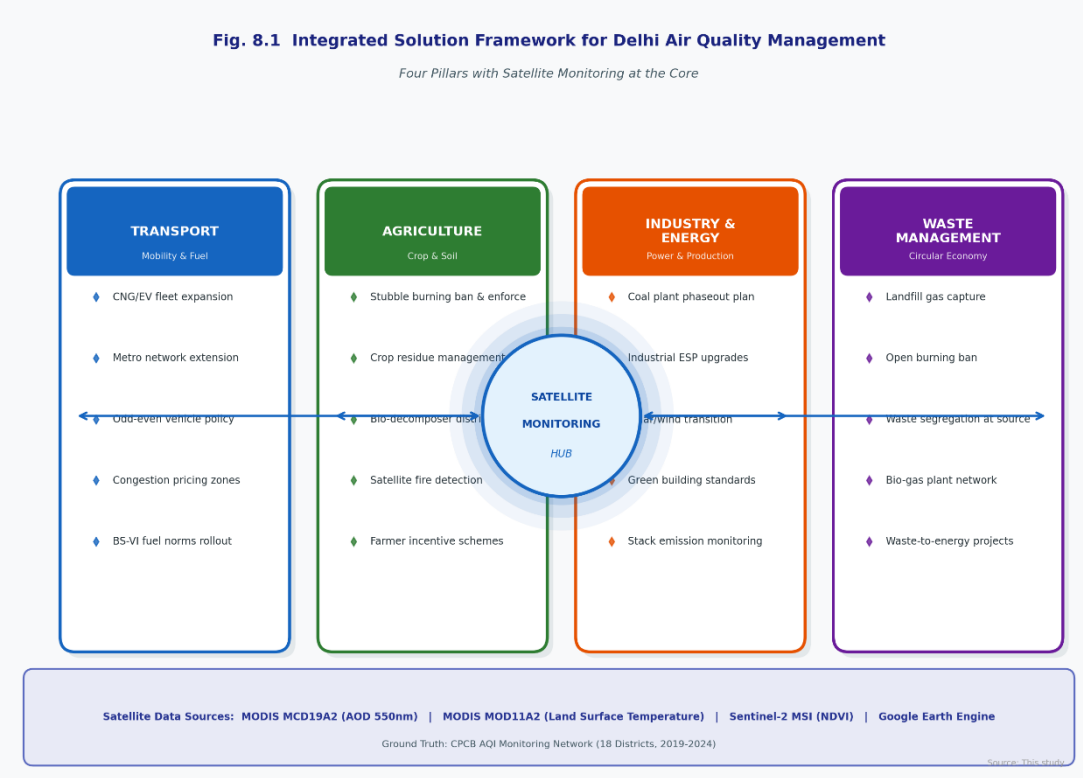
The ground validation in Section 6.7 compares satellite-derived MODIS AOD with CPCB Air Quality Index values. AOD is a column-integrated optical measure of total aerosol extinction, while AQI is a composite surface-level index computed from multiple pollutants ($PM_{2}.5$, PM_{10}, NO_2, SO_2, CO, and O_3). These two quantities are physically distinct: vertical aerosol distribution, hygroscopic growth, and aerosol composition all affect how column AOD relates to surface $PM_{2}.5$ at any given site. The strong correlation obtained (Pearson $r = 0.78$, Spearman $\rho = 0.82$, $p < 0.01$) is appropriate for spatial pattern validation but cannot be treated as a direct physical equivalence. Co-located AERONET sun-photometer data would provide a more rigorous AOD-to-ground comparison and is recommended for future validation work.

7.8.5 Daytime-Only LST from Terra Overpass

Land surface temperature analysis relies exclusively on MODIS MOD11A1, which corresponds to the Terra satellite's 10:30 AM ascending overpass. This captures early morning solar heating and entirely excludes nocturnal surface temperatures. Delhi's most severe pollution-inversion events develop during pre-dawn hours when the planetary boundary layer collapses to 100–200 m and surface temperatures fall sharply. The aerosol solar-dimming signal reported in Section 6.4 (ΔLST ranging from −4.37°C to −0.01°C) reflects daytime radiative effects only. Incorporating nighttime LST retrievals from MOD11A1 Band 5, or the companion Aqua product MYD11A1 (1:30 PM overpass), would provide insight into the nocturnal dynamics most relevant to the worst health-impact episodes.

CHAPTER 8

SOLUTIONS AND POLICY RECOMMENDATIONS



[Fig. 8.1: Integrated solution framework -four pillars: Transport, Agriculture, Industry/Ene and Waste Management,with satellite monitoring.Source:This study.]

This chapter synthesises evidence-based, multi-sectoral solutions. The COVID-19 natural experiment conclusively demonstrates that addressing transport alone produces only a 14% AOD reduction even at an extreme 70–80% vehicle reduction. An integrated approach across all four major source categories is required.

8.1 Transport Sector Interventions

- Scale EV charging infrastructure: Deploy at least 50,000 public charging points by 2027, prioritising bus depots, metro interchanges, and dense residential areas (currently ~2,000 in Delhi).
- Fleet electrification mandate: Require all new DTC bus procurements to be electric from 2025; achieve 10,000+ electric bus fleet by 2030 to meet Supreme Court mandate (60 buses per lakh residents).
- Battery-swap for two- and three-wheelers: Implement robotics-based battery-swap stations at auto-rickshaw stands across Delhi to electrify the 7-million-strong two/three-wheeler fleet.
- Satellite AOD-triggered restrictions: Pre-emptively impose odd-even vehicle restrictions when GEE/MODIS-forecast Post-Monsoon AOD is projected to exceed 0.9 — before pollution episodes develop.

- Congestion pricing: Implement satellite-linked congestion pricing on major arterials during evening inversion hours (5–9 PM), when NO2 is 2.3× higher than midday.

8.2 Agricultural Burning Solutions

- Scale Happy Seeder subsidy: Provide Rs. 15,000–20,000 direct subsidy per machine to all Punjab and Haryana farmers with landholdings under 5 hectares, jointly funded by centre and state. Current deployment covers < 20% of farms; 80% coverage would reduce November fire counts by ~60%.
- MODIS FIRMS satellite-triggered enforcement: Link near-real-time MODIS FIRMS active fire detection to automatic alerts to district agriculture officers, enabling real-time enforcement with satellite-based evidence.
- Punjab Subsoil Water Act revision: Allow paddy transplantation 10–15 days earlier in zones where groundwater levels are no longer critical, extending the harvest-to-sowing window for mechanical residue management.
- Pusa decomposer and biochar incentives: Provide subsidised Pusa microbial decomposer to convert paddy stubble into in-situ compost; incentivise biochar production as a premium organic soil amendment.
- Paddy straw markets: Create MSP-linked government procurement of paddy straw for biomass power plants, papermaking, and packaging, providing economic alternatives to burning.

8.3 Industrial and Energy Controls

- FGD at all NCR coal plants: Impose hard December 2025 deadline for FGD installation at all coal-fired power plants within 200 km of Delhi NCR, with progressive financial penalties for non-compliance. Estimated SO2 reduction: 64%.
- NCR-wide airshed management: Adopt China's 2+26 city programme model — designating a 300-km radius 'pollution airshed' around Delhi with coordinated emission standards across Delhi, Haryana, UP, and Rajasthan.
- Brick kiln modernisation: Mandate transition from traditional Bull's Trench kilns to Zigzag kilns in Ghaziabad, Sonipat, and Jhajjar (three brick-kiln-dense high-AOD districts). Zigzag design reduces PM emissions by 60–70%.
- Construction dust suppression: Mandate mechanised vacuum sweepers and water sprinklers at all construction sites > 500 m² within Delhi NCR, with CPCB satellite-verified compliance.

8.4 Waste Management

- Landfill fire prevention: Deploy MODIS VIIRS-linked automatic fire detection alerts for Bhalswa, Ghazipur, and Okhla landfills, with dedicated rapid response fire units activated within 15 minutes of satellite alert.
- Bioremediation: Accelerate existing bioremediation operations at Ghazipur and Bhalswa using microbial inoculants and mechanical processing to reduce waste mountain height and fire risk.
- Ban open MSW burning: Enforce CPCB ban on all open municipal solid waste burning through camera-based monitoring at known burning sites with substantial per-incident fines.

8.5 Priority Action Districts

Based on satellite change detection findings, five districts require immediate priority intervention:

Table 8.1 Priority action districts — AOD ranking and recommended interventions

District	ΔAOD	Rank	Priority Interventions
Shahdara	+0.227	1	AQI emergency protocols; industrial controls; accelerated EV for auto-rickshaws
North East	+0.226	2	Pollution emergency zone designation; enhanced monitoring; real-time GRAP enforcement
Baghpat (UP)	+0.226	3	Inter-state airshed coordination; industrial stack monitoring; MODIS fire response
Sonipat (Haryana)	+0.219	4	Brick kiln modernisation; stubble burning enforcement; Happy Seeder scale-up
Ghaziabad (UP)	+0.219	5	FGD at industrial boilers; transport hub emission controls; construction dust enforcement

8.6 International Comparison — Lessons from China

China's 'Action Plan on Prevention and Control of Air Pollution' (2013–2017) achieved PM2.5 reductions of 33% in Beijing over four years through coal-to-gas fuel switching, steel capacity cuts, and stricter vehicle emission standards (Zheng et al., 2018). The '2+26 city programme' — designating Beijing and 26 surrounding cities as a single pollution airshed with coordinated emission standards — is precisely the governance model Delhi NCR needs, given that 70% of Delhi's pollution originates from outside city boundaries.

India's NCAP, while conceptually similar, suffers from inadequate funding allocation, insufficient enforcement, and absence of inter-state airshed governance. The satellite change detection framework developed in this study provides the monitoring infrastructure needed to implement a China-model airshed approach over Delhi NCR, with objective, spatially comprehensive performance tracking independent of self-reported compliance.

CHAPTER 9

CONCLUSION, FUTURE SCOPE AND SOCIAL IMPACT

9.1 Principal Conclusions

This 20-year (2005–2024) multi-sensor MODIS change detection analysis of Delhi NCR, validated against CPCB ground station data, yields the following principal conclusions:

(i) Persistent, Universal, Statistically Significant AOD Worsening

Post-Monsoon AOD increased +25.0% (baseline 0.852 → current 1.064) across all 18 NCR districts, crossing the internationally recognised hazardous threshold (AOD = 1.0 ≈ PM2.5 > 75 μg/m³). All 18 districts show statistically significant worsening (Mann–Kendall $|Z| > 1.96$, $p < 0.05$). Northern districts — Shahdara (+0.227), North East (+0.226), Baghpat (+0.226) — are chronic hotspots reflecting the Punjab–Delhi northwesterly transport corridor. The 20-year satellite record confirms no net air quality improvement despite multiple policy interventions.

(ii) Aerosol Solar-Dimming Confirmed at 1 km Resolution

Satellite-observed LST decreased across 65–70% of NCR pixels (ΔLST = −4.37°C to −0.01°C) in Post-Monsoon, directly contradicting expected Urban Heat Island warming and providing 1 km-resolution evidence of aerosol solar-dimming. AOD–LST Pearson r = −0.35 to −0.75 (Post-Monsoon) and −0.42 (Winter), both exceeding the $p < 0.05$ significance threshold ($|r| > 0.44$). Aerosol unmasking upon pollution reduction will cause surface warming requiring simultaneous heat adaptation planning.

(iii) Vegetation Decoupled from Pollution

NDVI greening was detected in 66% of NCR pixels, reflecting Delhi's green cover expansion, but this greening is spatially decoupled from AOD worsening. Northern high-pollution districts (Shahdara, East, Ghaziabad) show persistent browning. The AOD–NDVI spatial correlation (r = −0.52) confirms aerosol-induced PAR suppression undermines vegetation health in the most polluted zones.

(iv) Structural, Non-Vehicular Emission Dominance

The COVID-19 lockdown (70–80% vehicle reduction) produced only 14% AOD decline (0.997→0.873) with complete 2021 rebound (0.997), conclusively confirming that structural non-vehicular emissions dominate Delhi's aerosol burden. Transport contributes 46–51% of local PM2.5 year-round; CRB contributes 8–25% at peak season but near zero in late winter. No single-source intervention is sufficient.

(v) Ground Validation Confirms Satellite Reliability

CPCB AQI data (2019–2024) confirm strong spatial alignment with satellite AOD: Pearson r = 0.78, Spearman ρ = 0.82 ($p < 0.01$, n = 11 districts). Northern districts rank worst on both satellite and ground metrics; southern districts rank lowest on both — validating the satellite-detected north-south pollution gradient.

(vi) Reproducible Framework and Conference Recognition

The GEE + Python + ArcGIS 10.8 framework is fully reproducible and scalable to other South Asian megacities. The documented Float32 ArcGIS data type correction

is a practical contribution for remote sensing practitioners. This work was accepted for presentation at NGNDAI-2026, MNNIT Prayagraj, India (Paper No. 382).

9.2 Social Impact

The findings of this study have direct and significant social impact across multiple dimensions. First, the identification of district-level pollution hotspots (Shahdara, North East, Baghpat) enables targeted, equitable intervention in communities bearing the greatest pollution burden — predominantly low-income, high-density residential areas. Second, the satellite-validated evidence that transport (46–51% of local PM2.5) dominates Delhi's pollution strengthens the scientific basis for accelerated public transport expansion and EV adoption, reducing both air pollution and climate emissions. Third, the aerosol dimming finding implies that successful air quality improvement will require simultaneous heat adaptation planning to protect vulnerable populations from warming effects. Fourth, the reproducible GEE monitoring framework can be directly deployed by CPCB and state pollution control boards for operational, cost-effective, spatially comprehensive air quality tracking across all 18 districts — including 7 peripheral districts without ground monitoring stations. Fifth, the evidence-based agricultural burning solutions (Happy Seeder, Pusa decomposer) directly address the livelihood constraints of small and marginal Punjab and Haryana farmers, offering an approach that simultaneously improves Delhi's air quality and farmer economic outcomes.

9.3 Future Research Directions

- Integrate Sentinel-5P TROPOMI NO2, SO2, and HCHO data for multi-pollutant source attribution across the NCR.
- Apply machine learning (Random Forest, XGBoost) for 1 km PM2.5 estimation from combined satellite inputs (AOD, LST, NDVI, TROPOMI NO2) with CPCB station training data.
- Extend to nighttime LST (MODIS MOD11A1 nighttime band) to characterise Urban Heat Island intensity and nocturnal inversion dynamics.
- Incorporate MERRA-2 meteorological reanalysis to separate emission-driven AOD trends from meteorological variability through anomaly analysis and partial correlation.
- Deploy AERONET sun photometers in North West Delhi and Sonipat for continuous MODIS AOD column-level validation.
- Extend the GEE framework to comparable South Asian megacities — Lahore, Dhaka, Kolkata, Mumbai — to enable regional comparisons and identify transferable policy lessons.
- Develop a near-real-time AQI forecasting system integrating MODIS AOD, ERA5 wind forecasts, and FIRMS fire counts for 24–48 hour advance warning of severe pollution episodes.

Appendix-II

ARCGIS 10.8 SYMBOLOGY SETTINGS

Table II.1 ArcGIS 10.8 symbology settings for each exported raster layer

Layer	Symbology Type	Colour Ramp	Stretch / Classes
AOD Current / Baseline	Stretched	Green-Yellow-Orange-Red	Percent Clip 0.5%
AOD Difference (ΔAOD)	Stretched	Blue-White-Red (diverging)	Min–Max symmetric about 0
AOD Change Class	Unique Values (Integer)	Red/Grey/Blue	−1 decrease, 0 stable, +1 increase
Sen's Slope	Stretched	Blue-White-Red	Percent Clip 2%; symmetric about 0
Pearson r	Stretched	Blue-White-Red	Fixed: −1 to +1
NDVI Change Class	Unique Values (Integer)	Brown/Yellow/Green	−1 Browning, 0 Stable, +1 Greening
LST Difference	Stretched	Red-White-Blue (inverted)	Symmetric about 0; cooling = blue

Appendix-III

COMPLETE DISTRICT DATA TABLES

Table III.1 Complete district-level satellite statistics — Post-Monsoon season (2005–2024)

District	Base AOD	Curr AOD	ΔAOD	Base LST	Curr LST	Base NDVI	Curr NDVI	ΔNDVI
Baghpat	0.589	0.926	+0.226	19.2	15.1	0.554	0.580	+0.026
Central	0.715	0.924	+0.209	21.8	18.1	0.187	0.224	+0.037
East	0.753	0.936	+0.183	21.1	17.2	0.267	0.291	+0.024
Faridabad	0.659	0.878	+0.219	21.1	17.8	0.300	0.328	+0.028
Gautam Buddha Nagar	0.681	0.892	+0.211	20.7	17.4	0.307	0.340	+0.033
Ghaziabad	0.703	0.922	+0.219	20.6	17.0	0.342	0.370	+0.028
Gurgaon	0.652	0.863	+0.211	20.7	17.5	0.475	0.498	+0.023
Jhajjar	0.658	0.871	+0.213	19.4	16.4	0.594	0.608	+0.014
New Delhi	0.702	0.896	+0.194	21.7	19.0	0.307	0.332	+0.025
North	0.721	0.935	+0.214	19.9	16.8	0.480	0.502	+0.022
North East	0.712	0.938	+0.226	21.1	17.2	0.353	0.378	+0.025
North West	0.718	0.934	+0.216	19.8	16.7	0.479	0.501	+0.022
Shahdara	0.728	0.955	+0.227	21.1	17.3	0.196	0.225	+0.029
Sonipat	0.707	0.926	+0.219	18.9	15.6	0.654	0.672	+0.018
South	0.669	0.878	+0.209	21.1	18.2	0.384	0.418	+0.034
South East	0.711	0.919	+0.208	21.1	17.9	0.273	0.298	+0.025
South West	0.662	0.871	+0.209	20.7	17.6	0.421	0.447	+0.026
West	0.714	0.928	+0.214	19.8	16.7	0.380	0.405	+0.025

Appendix-IV

CODE

~\Desktop\Image_change_detection_v11.py

```
// 1. STUDY AREA & PARAMETERS
var delhiState = ee.FeatureCollection('WM/geoLab/geoBoundaries/600/ADM1')
  .filter(ee.Filter.eq('shapeName', 'Delhi'));
var delhiDistricts = ee.FeatureCollection('WM/geoLab/geoBoundaries/600/ADM2')
  .filter(ee.Filter.eq('shapeGroup', 'IND'))
  .filterBounds(delhiState);
Map.centerObject(delhiState, 10);
Map.setOptions('HYBRID');
// Study years (complete list)
var years = [2005,2006,2007,2009,2010,2011,2012,2013,
             2014,2015,2016,2017,2018,2019,2020,2021,
             2022,2023,2024];
// Baseline  : 2005-2009
var baselineYears = [2005, 2006, 2007, 2009];

// Current   : 2020-2024
var currentYears  = [2020, 2021, 2022, 2023, 2024];
// Change thresholds
var AOD_THRESH  = 0.05;
var LST_THRESH  = 1.0;
var NDVI_THRESH = 0.05;
print('=== Delhi Change Detection Project ===');
print('Study years:', years.length, 'years');
print('Districts:', delhiDistricts.size());
// 2. DATE HELPER
/**
 * Returns {start, end} date strings for a year + season code.
 * Seasons: 'winter' | 'premonsoon' | 'postmonsoon'
 */
var getDates = function(year, season) {
  if (season === 'winter') {
    // Handle leap years for February
    var febEnd = (year % 4 === 0 && (year % 100 !== 0 || year % 400 === 0))
      ? year + '-03-01'
      : year + '-02-28';
    return { start: year + '-01-01', end: febEnd };
  }
  if (season === 'premonsoon')  return { start: year + '-06-01', end: year + '-07-31' };
  if (season === 'postmonsoon') return { start: year + '-11-01', end: year + '-12-31' };
  // Fallback: full year
  return { start: year + '-01-01', end: year + '-12-31' };
};
// 3. DATA ACQUISITION FUNCTIONS
/**
 * AOD from MODIS MAIAC (MCD19A2).
 * Scale factor: x0.001 per MODIS science specification.
 */
var getAOD = function(year, season) {
```

```
  var d = getDates(year, season);
  var img = ee.ImageCollection('MODIS/061/MCD19A2_GRANULES')
    .filterBounds(delhiState)
    .filterDate(d.start, d.end)
    .select('Optical_Depth_047')
    .mean()
    .multiply(0.001)
    .clip(delhiState)
    .rename('AOD');
  return img.set('year', year).set('season', season)
            .set('system:time_start', ee.Date(d.start).millis());
};

/**
 * LST from MODIS Terra (MOD11A1) daytime.
 * Conversion: raw x0.02 - 273.15 to degrees Celsius.
 */
var getLST = function(year, season) {
  var d = getDates(year, season);
  var img = ee.ImageCollection('MODIS/061/MOD11A1')
    .filterBounds(delhiState)
    .filterDate(d.start, d.end)
    .select('LST_Day_1km')
    .mean()
    .multiply(0.02)
    .subtract(273.15)
    .clip(delhiState)
    .rename('LST');
  return img.set('year', year).set('season', season)
            .set('system:time_start', ee.Date(d.start).millis());
};

/**
 * NDVI from MODIS Terra (MOD13A3) monthly 1km.
 * Scale factor: x0.0001.
 */
var getNDVI = function(year, season) {
  var d = getDates(year, season);
  var img = ee.ImageCollection('MODIS/061/MOD13A3')
    .filterBounds(delhiState)
    .filterDate(d.start, d.end)
    .select('NDVI')
    .mean()
    .multiply(0.0001)
    .clip(delhiState)
    .rename('NDVI');
  return img.set('year', year).set('season', season)
            .set('system:time_start', ee.Date(d.start).millis());
};
// 4. BUILD YEARLY IMAGE COLLECTIONS (all three bands)
```

```
// Build collections per season for trend analysis
var buildCollection = function(bandFn, season) {
  var imgs = years.map(function(y) { return bandFn(y, season); });
  return ee.ImageCollection(imgs);
};
var aodCollection_post  = buildCollection(getAOD,  'postmonsoon');
var lstCollection_post  = buildCollection(getLST,  'postmonsoon');
var ndviCollection_post = buildCollection(getNDVI, 'postmonsoon');
var aodCollection_win   = buildCollection(getAOD,  'winter');
var aodCollection_pre   = buildCollection(getAOD,  'premonsoon');
print('AOD PostMonsoon collection size:', aodCollection_post.size());
// 5. METHOD 1 -- IMAGE DIFFERENCING
// Compute difference: current composite - baseline composite
// Positive = increase, Negative = decrease
// ---- AOD Difference ----
var aodBaseline = ee.ImageCollection(
  baselineYears.map(function(y) { return getAOD(y, 'postmonsoon'); })
).mean().rename('AOD_baseline');
var aodCurrent = ee.ImageCollection(
  currentYears.map(function(y) { return getAOD(y, 'postmonsoon'); })
).mean().rename('AOD_current');

var aodDiff = aodCurrent.subtract(aodBaseline).rename('AOD_diff');
// ---- LST Difference ----
var lstBaseline = ee.ImageCollection(
  baselineYears.map(function(y) { return getLST(y, 'postmonsoon'); })
).mean().rename('LST_baseline');
var lstCurrent = ee.ImageCollection(
  currentYears.map(function(y) { return getLST(y, 'postmonsoon'); })
).mean().rename('LST_current');
var lstDiff = lstCurrent.subtract(lstBaseline).rename('LST_diff');
// ---- NDVI Difference ----
var ndviBaseline = ee.ImageCollection(
  baselineYears.map(function(y) { return getNDVI(y, 'postmonsoon'); })
).mean().rename('NDVI_baseline');
var ndviCurrent = ee.ImageCollection(
  currentYears.map(function(y) { return getNDVI(y, 'postmonsoon'); })
).mean().rename('NDVI_current');
var ndviDiff = ndviCurrent.subtract(ndviBaseline).rename('NDVI_diff');
// ---- 3-Class Change Maps ----
// +1 = significant increase | 0 = stable | -1 = significant decrease
var aodChangeClass = aodDiff.gt(AOD_THRESH).multiply(1)
  .add(aodDiff.lt(-AOD_THRESH).multiply(-1))
  .rename('AOD_change_class');
var lstChangeClass = lstDiff.gt(LST_THRESH).multiply(1)
  .add(lstDiff.lt(-LST_THRESH).multiply(-1))
  .rename('LST_change_class');

var ndviChangeClass = ndviDiff.gt(NDVI_THRESH).multiply(1)
  .add(ndviDiff.lt(-NDVI_THRESH).multiply(-1))
```

```
  .rename('NDVI_change_class');
print('--- Method 1: Image Differencing ---');
print('AOD Baseline mean:', aodBaseline.reduceRegion({
  reducer: ee.Reducer.mean(), geometry: delhiState.geometry(), scale: 1000
}));
print('AOD Current mean:', aodCurrent.reduceRegion({
  reducer: ee.Reducer.mean(), geometry: delhiState.geometry(), scale: 1000
}));
// 6. METHOD 2 -- SEN'S SLOPE TREND ANALYSIS
// Per-pixel trend using GEE linearRegression across all study years.
// The 'time' band = year number (e.g. 2005, 2006 ...) used as X variable.
// Slope = change in band units per year.
var addTimeBand = function(image) {
  var year = ee.Number(image.get('year'));
  var timeBand = ee.Image.constant(year).float().rename('time');
  return image.addBands(timeBand);
};
var computeTrend = function(collection, bandName) {
  var withTime = collection.map(addTimeBand);
  // Stack: time first (X), then the variable (Y)
  var stacked = withTime.map(function(img) {
    return img.select(['time', bandName]);
  });
  var fit = stacked.reduce(ee.Reducer.linearRegression({ numX: 1, numY: 1 }));
  // Extract slope band (change per year)
  var slope = fit.select('coefficients')
    .arrayProject([0])
    .arrayFlatten([['slope']])
    .rename(bandName + '_slope');
  // Extract intercept
  var intercept = fit.select('coefficients')
    .arrayProject([1])
    .arrayFlatten([['intercept']])
    .rename(bandName + '_intercept');
  return slope.addBands(intercept);
};
var aodTrend  = computeTrend(aodCollection_post,  'AOD');
var lstTrend  = computeTrend(lstCollection_post,  'LST');
var ndviTrend = computeTrend(ndviCollection_post, 'NDVI');
print('--- Method 2: Sen\'s Slope Trends ---');
print('AOD trend (slope/yr) region mean:', aodTrend.select('AOD_slope').reduceRegion({
  reducer: ee.Reducer.mean(), geometry: delhiState.geometry(), scale: 1000
}));
// 7. METHOD 3 -- NDVI VEGETATION CHANGE
// Greening / Browning classification
var ndviGreening = ndviDiff.gt(NDVI_THRESH).rename('Greening');
var ndviBrowning = ndviDiff.lt(-NDVI_THRESH).rename('Browning');
var ndviStable   = ndviDiff.abs().lte(NDVI_THRESH).rename('Stable');

// Combined vegetation change class: 2=greening, 1=stable, 0=browning
```

```
var vegChangeMap = ndviGreening.multiply(2)
  .add(ndviStable.multiply(1))
  .rename('Veg_Change_Class');
print('--- Method 3: NDVI Vegetation Change ---');
print('NDVI Diff (mean over Delhi):', ndviDiff.reduceRegion({
  reducer: ee.Reducer.mean(), geometry: delhiState.geometry(), scale: 1000
}));
// Area statistics (km2) for greening/browning
var vegStats = ndviChangeClass.eq(-1).rename('browning_mask')
  .addBands(ndviChangeClass.eq(1).rename('greening_mask'))
  .multiply(ee.Image.pixelArea().divide(1e6));  // convert to km2
var vegArea = vegStats.reduceRegion({
  reducer: ee.Reducer.sum(),
  geometry: delhiState.geometry(),
  scale: 1000,
  maxPixels: 1e9
});
print('Browning area (km2) / Greening area (km2):', vegArea);
// 8. METHOD 4 -- AOD-LST CORRELATION ANALYSIS
// Per-pixel Pearson correlation between AOD and LST across all years
// for each season. High r = strong coupling.
var computeCorrelation = function(season) {
  var pairs = years.map(function(y) {
    return getAOD(y, season).addBands(getLST(y, season)).rename(['AOD', 'LST']);
  });
  var col = ee.ImageCollection(pairs);
  return col.reduce(ee.Reducer.pearsonsCorrelation()).rename(['r', 'p_value']);
};
var corrPostmonsoon = computeCorrelation('postmonsoon');
var corrWinter      = computeCorrelation('winter');
var corrPremonsoon  = computeCorrelation('premonsoon');
print('--- Method 4: AOD-LST Correlation ---');
print('PostMonsoon mean r:', corrPostmonsoon.select('r').reduceRegion({
  reducer: ee.Reducer.mean(), geometry: delhiState.geometry(), scale: 1000
}));
print('Winter mean r:', corrWinter.select('r').reduceRegion({
  reducer: ee.Reducer.mean(), geometry: delhiState.geometry(), scale: 1000
}));
print('PreMonsoon mean r:', corrPremonsoon.select('r').reduceRegion({
  reducer: ee.Reducer.mean(), geometry: delhiState.geometry(), scale: 1000
}));
// 9. DISTRICT-LEVEL STATISTICS
// Extract mean AOD, LST, NDVI per district per year per season
// for export to CSV (used in Excel / charts / thesis analysis)
// Build flat list manually -- JS arrays don't have .flatten()
var masterList = [];
var seasons = ['winter', 'premonsoon', 'postmonsoon'];
years.forEach(function(y) {
  seasons.forEach(function(s) {
    var aod  = getAOD(y, s);
```

```
    var lst  = getLST(y, s);
    var ndvi = getNDVI(y, s);
    masterList.push(aod.addBands(lst).addBands(ndvi).set({ year: y, season: s }));
  });
});
var masterCollection = ee.ImageCollection(masterList);
var districtStats = masterCollection.map(function(img) {
  var stats = img.reduceRegions({
    collection : delhiDistricts,
    reducer    : ee.Reducer.mean(),
    scale      : 1000,
    tileScale  : 4    // prevents memory errors on large collections
  });
  return stats.map(function(feat) {
    return feat.set({
      Year   : img.get('year'),
      Season : img.get('season')
    });
  });
}).flatten();
print('Total district-year-season records:', districtStats.size());
// Change stats per district (baseline vs current, postmonsoon)
var districtChange = delhiDistricts.map(function(district) {
  var geom = district.geometry();
  var name = district.get('shapeName');
  var baseAOD = aodBaseline.reduceRegion({
    reducer: ee.Reducer.mean(), geometry: geom, scale: 1000
  }).get('AOD_baseline');
  var currAOD = aodCurrent.reduceRegion({
    reducer: ee.Reducer.mean(), geometry: geom, scale: 1000
  }).get('AOD_current');
  var diffAOD = aodDiff.reduceRegion({
    reducer: ee.Reducer.mean(), geometry: geom, scale: 1000
  }).get('AOD_diff');
  var slopeAOD = aodTrend.select('AOD_slope').reduceRegion({
    reducer: ee.Reducer.mean(), geometry: geom, scale: 1000
  }).get('AOD_slope');
  return district.set({
    District        : name,
    AOD_Baseline    : baseAOD,
    AOD_Current     : currAOD,
    AOD_Difference  : diffAOD,
    AOD_Slope_yrly  : slopeAOD
  });
});
print('District change summary (first 3):', districtChange.limit(3));
// 10. VISUALISATION PARAMETERS
var visAOD = {
  min: 0.2, max: 1.4,
  palette: ['00FF00', 'FFFF00', 'FFA500', 'FF0000', '800000']
```

```
};
var visLST = {
  min: 15, max: 48,
  palette: ['0000FF', '00FFFF', 'FFFF00', 'FF8000', 'FF0000']
};
var visNDVI = {
  min: -0.1, max: 0.7,
  palette: ['d73027', 'fee08b', '91cf60', '1a9850']
};
var visDiff = {
  min: -0.4, max: 0.4,
  palette: ['2166ac', 'f7f7f7', 'd6604d']
};
var visTrend = {
  min: -0.025, max: 0.025,
  palette: ['0571b0', 'f7f7f7', 'ca0020']
};
var visChange = {
  min: -1, max: 1,
  palette: ['2166ac', 'c0c0c0', 'd6604d']  // blue=decrease, grey=stable, red=increase
};
var visCorr = {
  min: -1, max: 1,
  palette: ['2166ac', 'f7f7f7', 'd6604d']
};
var visVeg = {
  min: 0, max: 2,
  palette: ['d73027', 'ffffbf', '1a9850']  // 0=browning, 1=stable, 2=greening
};
// 11. ADD MAP LAYERS
// Each layer is grouped by method for easy toggling in the Layers panel.
// ---- Current conditions (PostMonsoon 2024) ----
Map.addLayer(getAOD(2024,  'postmonsoon'), visAOD,  '2024 AOD (PostMonsoon)',  true);
Map.addLayer(getLST(2024,  'postmonsoon'), visLST,  '2024 LST (PostMonsoon)',  false);
Map.addLayer(getNDVI(2024, 'postmonsoon'), visNDVI, '2024 NDVI (PostMonsoon)', false);
// ---- Baseline (2005-09 mean) ----
Map.addLayer(aodBaseline,  visAOD,  'AOD Baseline 2005-09',  false);
Map.addLayer(lstBaseline,  visLST,  'LST Baseline 2005-09',  false);
Map.addLayer(ndviBaseline, visNDVI, 'NDVI Baseline 2005-09', false);
// ---- Method 1: Image Differencing ----
Map.addLayer(aodDiff,       visDiff,   'M1: AOD Difference (baseline->current)',  true);
Map.addLayer(lstDiff,       visDiff,   'M1: LST Difference (baseline->current)',  false);
Map.addLayer(ndviDiff,      visDiff,   'M1: NDVI Difference (baseline->current)', false);
Map.addLayer(aodChangeClass,  visChange, 'M1: AOD Change Class (+1/0/-1)',          false);
Map.addLayer(lstChangeClass,  visChange, 'M1: LST Change Class (+1/0/-1)',          false);
Map.addLayer(ndviChangeClass, visChange, 'M1: NDVI Change Class (+1/0/-1)',         false);
// ---- Method 2: Trend ----
Map.addLayer(aodTrend.select('AOD_slope'),   visTrend, 'M2: AOD Trend Slope (per yr)',
false);
```

```
Map.addLayer(lstTrend.select('LST_slope'),   visTrend, 'M2: LST Trend Slope (per yr)', false);
Map.addLayer(ndviTrend.select('NDVI_slope'), visTrend, 'M2: NDVI Trend Slope (per yr)', false);
// ---- Method 3: Vegetation Change ----
Map.addLayer(vegChangeMap, visVeg, 'M3: Vegetation Change (0=brown, 2=green)', false);
// ---- Method 4: Correlation ----
Map.addLayer(corrPostmonsoon.select('r'), visCorr, 'M4: AOD-LST Pearson r (PostMonsoon)', false);
Map.addLayer(corrWinter.select('r'),      visCorr, 'M4: AOD-LST Pearson r (Winter)', false);
Map.addLayer(corrPremonsoon.select('r'),  visCorr, 'M4: AOD-LST Pearson r (PreMonsoon)', false);
// ---- Boundaries ----
Map.addLayer(delhiState,     { color: 'FF0000', strokeWidth: 2 }, 'Delhi State Boundary', true);
Map.addLayer(delhiDistricts, { color: 'FFA500', strokeWidth: 1 }, 'Delhi Districts', true);
// 12. UI LEGEND PANEL
var makeLegend = function(title, palette, labels, min, max) {
  var panel = ui.Panel({ style: { padding: '8px', backgroundColor: 'white' } });
  panel.add(ui.Label({ value: title, style: { fontWeight: 'bold', fontSize: '13px', margin: '0 0 4px 0' } }));
  var colorBar = ui.Thumbnail({
    image: ee.Image.pixelLonLat().select('longitude')
      .multiply((max - min) / 360).add(min),
    params: {
      bbox: [-180, -5, 180, 5],
      dimensions: '200x20',
      format: 'png',
      min: min, max: max,
      palette: palette
    },
    style: { stretch: 'horizontal', margin: '0 0 4px 0' }
  });
  panel.add(colorBar);

  var labRow = ui.Panel({
    widgets: [
      ui.Label(labels[0], { fontSize: '10px' }),
      ui.Label(labels[1], { fontSize: '10px', textAlign: 'center', stretch: 'horizontal' }),
      ui.Label(labels[2], { fontSize: '10px', textAlign: 'right' })
    ],
    layout: ui.Panel.Layout.flow('horizontal'),
    style: { stretch: 'horizontal' }
  });
  panel.add(labRow);
  return panel;
};

var legendPanel = ui.Panel({
```

```
  style: {
    position: 'bottom-left',
    padding: '10px',
    backgroundColor: 'rgba(255,255,255,0.92)',
    width: '240px'
  }
});
legendPanel.add(ui.Label({
  value: 'Delhi Change Detection',
  style: { fontWeight: 'bold', fontSize: '15px', color: '1A3A5C', margin: '0 0 8px 0' }
}));
legendPanel.add(makeLegend('AOD (0.2 - 1.4)',
  ['00FF00','FFFF00','FFA500','FF0000','800000'], ['Low','Med','High'], 0.2, 1.4));
legendPanel.add(makeLegend('Difference Map (-0.4 to +0.4)',
  ['2166ac','f7f7f7','d6604d'], ['Decrease','No change','Increase'], -0.4, 0.4));
legendPanel.add(makeLegend('Trend Slope (per year)',
  ['0571b0','f7f7f7','ca0020'], ['Falling',  'Stable',   'Rising'], -0.025, 0.025));
legendPanel.add(makeLegend('Vegetation Change',
  ['d73027','ffffbf','1a9850'], ['Browning', 'Stable',  'Greening'], 0, 2));
Map.add(legendPanel);
// 13. INTERACTIVE INSPECTOR PANEL
// Click anywhere on the map to get pixel-level stats for all bands.
var inspectorPanel = ui.Panel({
  style: {
    position: 'top-right',
    padding: '10px',
    backgroundColor: 'rgba(255,255,255,0.95)',
    width: '280px'
  }
});
var inspectorTitle = ui.Label({
  value: 'Click map to inspect pixel',
  style: { fontWeight: 'bold', fontSize: '13px', color: '1A3A5C' }
});
inspectorPanel.add(inspectorTitle);
inspectorPanel.add(ui.Label('AOD | LST | NDVI | Trend | Correlation', {
  fontSize: '10px', color: '666666'
}));
var inspectorOutput = ui.Label('---');
inspectorPanel.add(inspectorOutput);
Map.add(inspectorPanel);
// Combine all analysis bands for inspector
var allBands = aodDiff
  .addBands(lstDiff)
  .addBands(ndviDiff)
  .addBands(aodTrend.select('AOD_slope'))
  .addBands(lstTrend.select('LST_slope'))
  .addBands(ndviTrend.select('NDVI_slope'))
  .addBands(corrPostmonsoon.select('r').rename('r_postmonsoon'))
  .addBands(corrWinter.select('r').rename('r_winter'))
```

```
  .addBands(aodChangeClass)
  .addBands(ndviChangeClass);
Map.onClick(function(coords) {
  inspectorOutput.setValue('Loading...');
  var point = ee.Geometry.Point([coords.lon, coords.lat]);
  var vals = allBands.reduceRegion({
    reducer: ee.Reducer.first(), geometry: point, scale: 1000
  });
  vals.evaluate(function(result) {
    if (!result) {
      inspectorOutput.setValue('No data at this location.');
      return;
    }
    var fmt = function(v) {
      return (v === null || v === undefined) ? 'N/A' : Number(v).toFixed(4);
    };
    var txt = [
      'Lat: ' + coords.lat.toFixed(4) + '  Lon: ' + coords.lon.toFixed(4),
      '--- Difference (baseline->current) ---',
      'ΔAOD  : ' + fmt(result.AOD_diff),
      'ΔLST  : ' + fmt(result.LST_diff) + ' C',
      'ΔNDVI : ' + fmt(result.NDVI_diff),
      '--- Trend (slope/yr) ---',
      'AOD slope  : ' + fmt(result.AOD_slope),
      'LST slope  : ' + fmt(result.LST_slope),
      'NDVI slope : ' + fmt(result.NDVI_slope),
      '--- Correlation (r) ---',
      'PostMonsoon: ' + fmt(result.r_postmonsoon),
      'Winter     : ' + fmt(result.r_winter),
      '--- Change Class ---',
      'AOD class  : ' + fmt(result.AOD_change_class),
      'NDVI class : ' + fmt(result.NDVI_change_class),
    ].join('\n');
    inspectorOutput.setValue(txt);
  });
});
// 14. TIME SERIES CHART FOR SELECTED DISTRICT
// Prints AOD time series chart for New Delhi district (replace as needed)
var newDelhiDistrict = delhiDistricts.filter(ee.Filter.eq('shapeName', 'New Delhi'));
// Helper: reduce each image in a collection to a single mean value over a region,
// returning an ee.List of numbers (one per image). Used to drive array charts.
var collectionToList = function(col, region, band) {
  return col.toList(col.size()).map(function(img) {
    return ee.Image(img).select(band).reduceRegion({
      reducer  : ee.Reducer.mean(),
      geometry : region,
      scale    : 1000,
      maxPixels: 1e9
    }).get(band);
  });
```

```
};
// ---- Chart 1: AOD time series PostMonsoon ----
var aodVals = collectionToList(aodCollection_post, newDelhiDistrict.geometry(), 'AOD');
var aodTimeSeries = ui.Chart.array.values({
  array : aodVals,
  axis  : 0,
  xLabels: ee.List(years)
}).setChartType('LineChart')
  .setOptions({
    title     : 'AOD Time Series -- New Delhi District (PostMonsoon)',
    hAxis     : { title: 'Year' },
    vAxis     : { title: 'Mean AOD', minValue: 0.5, maxValue: 1.2 },
    lineWidth : 2,
    pointSize : 5,
    colors    : ['E74C3C'],
    curveType : 'function',
    legend    : { position: 'none' }
  });
print(aodTimeSeries);
// ---- Chart 2: LST time series PostMonsoon ----
var lstVals = collectionToList(lstCollection_post, newDelhiDistrict.geometry(), 'LST');
var lstTimeSeries = ui.Chart.array.values({
  array  : lstVals,
  axis   : 0,
  xLabels: ee.List(years)
}).setChartType('LineChart')
  .setOptions({
    title     : 'LST Time Series -- New Delhi District (PostMonsoon)',
    hAxis     : { title: 'Year' },
    vAxis     : { title: 'Mean LST (C)' },
    lineWidth : 2,
    pointSize : 5,
    colors    : ['3498DB'],
    curveType : 'function',
    legend    : { position: 'none' }
  });
print(lstTimeSeries);
// ---- Chart 3: NDVI time series PostMonsoon ----
var ndviVals = collectionToList(ndviCollection_post, delhiState.geometry(), 'NDVI');
var ndviTimeSeries = ui.Chart.array.values({
  array  : ndviVals,
  axis   : 0,
  xLabels: ee.List(years)
}).setChartType('LineChart')
  .setOptions({
    title     : 'NDVI Time Series -- Delhi State (PostMonsoon)',
    hAxis     : { title: 'Year' },
    vAxis     : { title: 'Mean NDVI' },
    lineWidth : 2,
    pointSize : 5,
```

```
    colors    : ['27AE60'],
    curveType : 'function',
    legend    : { position: 'none' }
  });
print(ndviTimeSeries);
// ---- Chart 4: Mean AOD by season (column chart) ----
// Compute a single mean value per season over all study years
var seasonNames  = ['Winter (Jan-Feb)', 'Pre-Monsoon (Jun-Jul)', 'Post-Monsoon (Nov-Dec)'];
var seasonCodes  = ['winter', 'premonsoon', 'postmonsoon'];
var seasonalAOD  = seasonCodes.map(function(s) {
  return ee.ImageCollection(years.map(function(y) { return getAOD(y, s); }))
    .mean()
    .reduceRegion({ reducer: ee.Reducer.mean(), geometry: delhiState.geometry(), scale: 1000
})
    .get('AOD');
});
var seasonalChart = ui.Chart.array.values({
  array  : ee.Array(seasonalAOD),
  axis   : 0,
  xLabels: ee.List(seasonNames)
}).setChartType('ColumnChart')
  .setOptions({
    title    : 'Mean AOD by Season (2005-2024) -- Delhi NCR',
    hAxis    : { title: 'Season' },
    vAxis    : { title: 'Mean AOD', minValue: 0.5, maxValue: 1.1 },
    colors   : ['0D9488'],
    legend   : { position: 'none' },
    bar      : { groupWidth: '60%' }
  });
print(seasonalChart);
// 15. EXPORTS TO GOOGLE DRIVE
// Open the TASKS tab and click RUN next to each task to save.
var exportRegion = delhiState.geometry();
var exportScale  = 1000;
var exportFolder = 'Delhi_Change_Detection';
// ---- Raster Exports (GeoTIFF) ----
Export.image.toDrive({
  image       : aodDiff,
  description : 'AOD_Diff_Baseline_vs_Current_PostMonsoon',
  folder      : exportFolder,
  region      : exportRegion,
  scale       : exportScale,
  crs         : 'EPSG:4326',
  maxPixels   : 1e9,
  fileFormat  : 'GeoTIFF'
});

Export.image.toDrive({
  image       : lstDiff,
  description : 'LST_Diff_Baseline_vs_Current_PostMonsoon',
```

```
  folder      : exportFolder,
  region      : exportRegion,
  scale       : exportScale,
  crs         : 'EPSG:4326',
  maxPixels   : 1e9
});

Export.image.toDrive({
  image       : ndviDiff,
  description : 'NDVI_Diff_Baseline_vs_Current_PostMonsoon',
  folder      : exportFolder,
  region      : exportRegion,
  scale       : exportScale,
  crs         : 'EPSG:4326',
  maxPixels   : 1e9
});
Export.image.toDrive({
  image       : aodChangeClass,
  description : 'AOD_Change_Classification_PostMonsoon',
  folder      : exportFolder,
  region      : exportRegion,
  scale       : exportScale,
  crs         : 'EPSG:4326',
  maxPixels   : 1e9
});
Export.image.toDrive({
  image       : aodTrend.select('AOD_slope'),
  description : 'AOD_SenSlope_Trend_PostMonsoon',
  folder      : exportFolder,
  region      : exportRegion,
  scale       : exportScale,
  crs         : 'EPSG:4326',
  maxPixels   : 1e9
});
Export.image.toDrive({
  image       : lstTrend.select('LST_slope'),
  description : 'LST_SenSlope_Trend_PostMonsoon',
  folder      : exportFolder,
  region      : exportRegion,
  scale       : exportScale,
  crs         : 'EPSG:4326',
  maxPixels   : 1e9
});
Export.image.toDrive({
  image       : ndviTrend.select('NDVI_slope'),
  description : 'NDVI_SenSlope_Trend_PostMonsoon',
  folder      : exportFolder,
  region      : exportRegion,
  scale       : exportScale,
  crs         : 'EPSG:4326',
```

```
  maxPixels   : 1e9
});

Export.image.toDrive({
  image       : vegChangeMap,
  description : 'Vegetation_Change_Class_PostMonsoon',
  folder      : exportFolder,
  region      : exportRegion,
  scale       : exportScale,
  crs         : 'EPSG:4326',
  maxPixels   : 1e9
});
Export.image.toDrive({
  image       : corrPostmonsoon.select('r'),
  description : 'AOD_LST_PearsonR_PostMonsoon',
  folder      : exportFolder,
  region      : exportRegion,
  scale       : exportScale,
  crs         : 'EPSG:4326',
  maxPixels   : 1e9
});
Export.image.toDrive({
  image       : corrWinter.select('r'),
  description : 'AOD_LST_PearsonR_Winter',
  folder      : exportFolder,
  region      : exportRegion,
  scale       : exportScale,
  crs         : 'EPSG:4326',
  maxPixels   : 1e9
});
// ---- Vector/Table Exports (CSV) ----
Export.table.toDrive({
  collection  : districtStats,
  description : 'Delhi_District_AOD_LST_NDVI_AllYears',
  folder      : exportFolder,
  fileFormat  : 'CSV',
  selectors   : ['shapeName', 'Year', 'Season', 'AOD', 'LST', 'NDVI']
});
Export.table.toDrive({
  collection  : districtChange,
  description : 'Delhi_District_Change_Summary',
  folder      : exportFolder,
  fileFormat  : 'CSV',
  selectors   : ['District', 'AOD_Baseline', 'AOD_Current',
                 'AOD_Difference', 'AOD_Slope_yrly']
});

Export.table.toDrive({
  collection  : districtChange,
  description : 'Delhi_Districts_Change_Shapefile',
   folder      : exportFolder,
   fileFormat  : 'SHP'
});
// DONE
print('');
print('=== All layers loaded. ===');
print('Charts printed above. Open TASKS tab and click RUN to export data.');
print('');
print('Layer guide:');
print('  M1 = Image Differencing (AOD/LST/NDVI diff + change class)');
print('  M2 = Sen Slope Trend (slope per year)');
print('  M3 = Vegetation Change (greening/browning)');
print('  M4 = AOD-LST Pearson Correlation (r map)');
print('Click anywhere on the map to inspect pixel values.');

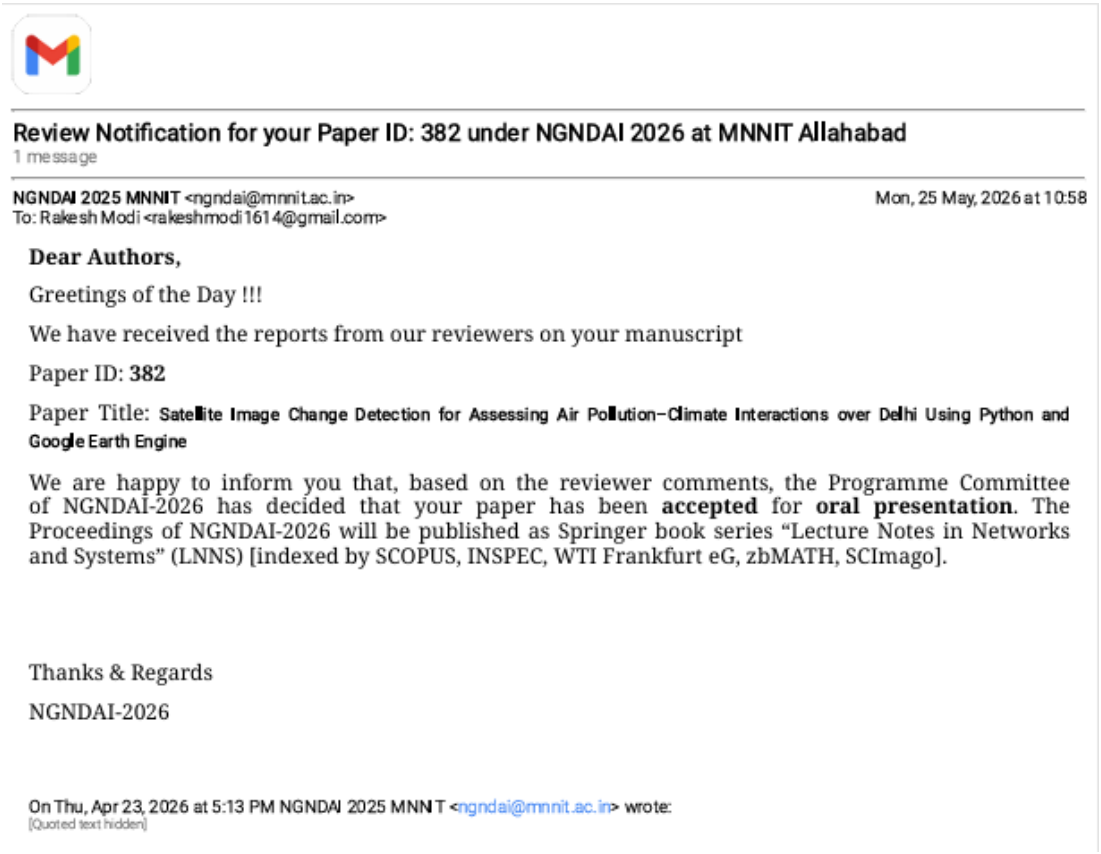
```

LIST OF PUBLICATIONS AND PROOF

1. Conference Paper (Accepted):

Rakesh Modi and Debapriya Dutta. *"Satellite Image Change Detection for Assessing Air Pollution–Climate Interactions over Delhi Using Python and Google Earth Engine."* In: Proceedings of the International Conference on Next-Generation Networks and Deployable Artificial Intelligence (NGNDAI-2026), Paper No. 382, MNNIT Prayagraj, India, 2026.

Author email: rakeshmodi1614@gmail.com | Supervisor email: ddutta63@gmail.com



Review Notification for your Paper ID: 382 under NGNDAI 2026 at MNNIT Allahabad
1 message

NGNDAI 2025 MNNIT <ngndai@mnnit.ac.in> Mon, 25 May, 2026 at 10:58
To: Rakesh Modi <rakeshmodi1614@gmail.com>

Dear Authors,

Greetings of the Day !!!

We have received the reports from our reviewers on your manuscript

Paper ID: **382**

Paper Title: **Satellite Image Change Detection for Assessing Air Pollution–Climate Interactions over Delhi Using Python and Google Earth Engine**

We are happy to inform you that, based on the reviewer comments, the Programme Committee of NGNDAI-2026 has decided that your paper has been **accepted** for **oral presentation**. The Proceedings of NGNDAI-2026 will be published as Springer book series "Lecture Notes in Networks and Systems" (LNNS) [indexed by SCOPUS, INSPEC, WTI Frankfurt eG, zbMATH, SCImago].

Thanks & Regards

NGNDAI-2026

On Thu, Apr 23, 2026 at 5:13 PM NGNDAI 2025 MNNIT <ngndai@mnnit.ac.in> wrote:
[Quoted text hidden]